MESHLESS MODELING OF WAVE INDUCED FLOWS INSIDE SANDY SEA BEDS

by

Burak Can Timuçin

B.S., Civil Engineering, State University of New York at Buffalo, 2011

B.S., Civil Engineering, Istanbul Technical University, 2012

Submitted to the Institute for Graduate Studies in
Science and Engineering in partial fulfillment of
the requirements for the degree of
Master of Science

Graduate Program in Computational Sciences and Engineering

Boğaziçi University

2015

To my family,

ACKNOWLEDGEMENTS

I would like to express my sincere gratitude to my thesis supervisor Assoc. Prof. Osman S. Börekçi for his invaluable guidance and help during the preparation of this thesis study. I would like to acknowledge his patience and his positive approach during the impasse moments of my studies.

I would like to express my thanks to my colleagues Cenk Güngör, Yiğit Can Altan, Ulvi Berat Şensoy for their help and support.

I would also like to express my thanks to Assoc. Prof. Emre Otay and Prof. Cem Avcı for their support and help during the preparation of this thesis.

Most of all, I would like to express my special thanks to my parents, my brother, my sister and to my wife for their endless support and encouragement they have given me throughout this period.

ABSTRACT

MESHLESS MODELING OF WAVE INDUCED FLOWS INSIDE SANDY SEA BEDS

Ocean waves have been research focus for scientists and engineers for the last several decades, being one of the most dominant physical phenomena that affect the coastal zones. Varieties of wave theories have been developed to understand the complex nature of this phenomenon. With the emergence of computers in the midst of twentieth century and the introduction of computational approach in science, ocean wave modeling has become an integral part of the studies on ocean waves. Among several numerical methods offered, developed and applied to the ocean wave problems, one of the most recent and practical is a meshless method called Radial Basis Function Collocation Method. The motivation behind the proposed modeling effort is the development of an understanding of how oxygen entrained in coastal waters penetrates into sandy sea bottoms. To understand the related phenomena, a linear wave propagation model over a porous sandy sea bed was developed using a meshless method, the Radial Basis Function Collocation Method (RBFCM). The Green's function of the Laplace equation was used as the Radial Basis Function (RBF). The solution of equations on the boundaries was used to obtain the values inside the solution domain using the RBF interpolation. The results indicate that the method used here, a boundary-only RBFCM solution, is an efficient method for solving the problem at hand.

ÖZET

KUMLU DENİZ TABANI İÇERİSİNDE DALGA ETKİSİYLE OLUŞAN AKIMLARIN AĞSIZ YÖNTEMLE MODELLEMESİ

Deniz dalgaları, kıyı alanlarını değiştiren en önemli doğal olgulardan biri olarak, son yıllarda bilim insanları ve mühendisler için ilgi çekici ve önemli bir çalışma alanı olmuştur. Konunun kompleks yapısını anlamak adına, bilim insanları bugüne kadar bir çok teori geliştirmiştirlerdir. Yirminci yüzyılın ortalarında, bilgisayarın ve hesaplamalı bilimlerin ortaya çıkmasıyla, deniz dalgalarının modellenmesi bu çalışmaların önemli bir parçası haline gelmiştir. Öne sürülen, geliştirilen ve uygulanan bir çok nümerik metod arasında, ağsız bir yöntem olan, Radyal Bazlı Kolokasyon Metodu en güncel ve uygulanması açısından en pratik olanları arasında yer almaktadır. Bu çalışmanın amacı, deniz suyu içerisinde bulunan eriyik oksijenin ve diğer organik maddelerin, dalga etkisiyle kumlu deniz tabanı içerisindeki taşınımını anlamak için gereken sayısal modelleme altyapısını oluşturmaktır. Bu amaçla, geçirimli ve kum dalgacıklı bir taban üzerinde lineer dalga ilerlemesi ağsız Radyal Bazlı Fonksiyon Kolokasyon Metodu (RBFKM) ile modellenmiştir. Problemin formülasyonunda sadece sınır şartlarını ifade denklemler kullanılmıştır. Akımı belirleyen süreklilik denklemi ise radyal bazlı fonksiyon (RBF) olarak Laplace denkleminin Green fonksiyonu kullanılarak formülasyona dahil edilmiştir. Çözüm sonucunda sınırlarda elde edilen akım potansiyeli değerleri, RBF enterpolasyonu kullanılarak, çözüm alanı içerisindeki noktalardaki değerlerin hesaplanmasında kullanılmıştır. Elde edilen bulgular, kullanılan sınır tipi RBFKM' nun problemin çözümü için uygun bir metod olduğunu göstermiştir.

TABLE OF CONTENTS

LIST OF FIGURES

LIST OF TABLES

LIST OF SYMBOLS

A	Wave amplitude
a_1	BVP coefficient
a_2	BVP coefficient
b_1	BVP coefficient
b_2	BVP coefficient
B	Boundary operator
c	Wave celerity
f	Radial Basis Function
g	Acceleration of gravity
h	Water depth
i	Matrix indices
j	Matrix indices
K	Permeability coefficient
k	Wave number
L	Wave length
L	Field operator
T	Wave period
u	X-component of velocity of the fluid particle
r	Radius

v	Y-component of velocity of the fluid particle
w	Z-component of velocity of the fluid particle
z	Water depth
ϕ	Velocity potential in sea zone
η	Free surface displacement
ρ	Density of water
ψ	Velocity potential in sand zone
∇	Gradient operator
∇^2	Laplace operator
ς	Coordinate indicator

LIST OF ACRONYMS/ABBREVIATONS

BIEM	Boundary Integral Element Method
MSE	Mild Slope Equations
RANS	Reynolds Averaged Navier-Stokes Equations
RBF	Radial Basis Function
RBFCM	Radial Basis Function Collocation Method
RMS	Root Mean Square Error
PLIC-VOF	Piecewise Linear Interface Construction - Volume of Fluid

1. INTRODUCTION

Coastal zones, where lands and oceans meet, are the geological environments that shape humanity's residency and way of living in this planet since the beginning of time. Coastal and ocean engineering have been an integral part of the humanity's investigation on these unique places from ancient times; yet, it is not older than several decades that significant advances have been accomplished in this area.

Being one of the most dominant physical phenomena that affect the coastal zones, ocean waves have been a research focus for scientists and engineers in the last several decades. Ocean wave problems have become a research area for coastal engineers, marine and offshore engineers, engineers working on naval structures and on design of ships, and scientists who are working on physical oceanography and marine hydrodynamics. Various wave theories on ocean waves have been developed which provided us the understanding of the physical mechanism of ocean waves. However; due to the complex nature of the ocean waves, a lot of research work have been based on linear or other simplified theories.

Ocean wave modeling efforts have became an important part of the studies mentioned above ever since the computational approach was introduced to the scientific world. Many numerical techniques has been offered, developed and applied to the ocean wave problems for a variety of needs. Recently, a new numerical method called meshless method is showing a rapid progress due to the great interest to the subject by computational scientists and coastal engineers. Unlike previous numerical methods at hand, meshless methods do not require the formation of a mesh neither inside the solution domain nor on the boundaries of the solution domain. Thus, meshless methods are proved to be effective while dealing with problems including moving boundaries or large deformations.

A meshless method called Radial Basis Function Collocation Method (RBFCM) is utilized in the study at hand. First introduced by E.J. Kansa (1990a, 1990b), RBFCM is a method to solve elliptic, hyperbolic and parabolic differential equations. The prominent characteristic of the RBFCM method is the flexibility while setting up the problem

geometry. More information on RBFCM and its application in this study will be given in the later chapters.

Wave motion on the sea surface induces flows inside the sea bed which allows organic materials and oxygen inside the sea water to be transported into the sea bed. This physical phenomenon is vital for the ecological system in oceans since micro-organisms and bacteria consume organic materials and oxygen to aid nutriment production process. The effectiveness of this process depends on the transportation of organic materials and oxygen inside the sea bed. This transportation process is, in brief, an advection diffusion process. The motivation behind this study is to develop a wave propagation model, using a different application of RBFCM, and investigate how flows inside a sandy and rippled sea bed are formed under waves. The models presented in this study, forms a basis to understand the transportation process described. There are four stages of the study at hand which are wave propagation over impermeable and horizontal sea bed, wave propagation over impermeable and rippled sea bed, wave propagation over permeable and horizontal sea bed and wave propagation over permeable and rippled sea bed.

The thesis is presented in six chapters. In the second chapter, an overview of past studies on wave theories and wave modeling related to our study case are presented. The third chapter presents the mathematical derivations of the wave propagation models developed. The fourth chapter introduces the RBFCM and clarifies the usage of RBFCM in this study. Numerical tests and results are presented in the fifth chapter and the sixth chapter covers the interpretation of these findings, also offers ideas for future studies.

2. LITERATURE SURVEY

Water wave propagation over permeable sea beds or coastal structures has been an interesting area of research for scientists over the years. Early works of these studies can be traced back to Putnam (1949) where a significant loss of wave energy due to the viscous percolation of fluid into the sand was investigated. Reid and Kajura (1957) re-examined the problem of percolation from the stand point of damped waves in a two layer, coupled system wherein the pressure and velocity distributions in the upper layer not only govern but are in turn influenced by the percolation in the permeable lower layer. In order to simplify the problem, Putnam (1949) and Reid and Kajura (1957) used the classical irrotational wave solution above a region of viscous porous flow, with continuity in pressure and vertical velocity at the interface. Hunt (1959) argued that, this approach leads to a solution in which there is a discontinuity in the horizontal component of the velocity at the interface, thus not representing the real situation very closely since the absence of sand movement along the sea bed would be an additional source of dissipation and viscous conditions require the horizontal component of velocity in the water to vanish at the sea bed. In his paper, a solution is proposed for the wave damping as a function of viscosity, permeability and porosity. Lui (1973) argued that Hunt's (1959) trial to improve the deficiency mentioned above is not successful since the discontinuity of the horizontal velocity still appears in the interface and the velocity components in the water remained unaffected by the permeable sea bed. In his paper, he used the unsteady Darcy's equation to model the flow in a permeable sea bed and determined the damping rate using the same boundary layer approach and the energy balance statement. Sollitt and Cross (1972) did a study on wave transformation through permeable breakwaters where a theory was derived to predict ocean wave reflection and transmission at a permeable breakwater. The theory solves for a damped wave component within the breakwater and matches the boundary conditions at the windward and leeward breakwater faces to predict the reflected and transmitted wave components.

An alternative theoretical model for the sea bed pressure response was proposed by Moshagen and Torum (1975), in which the main assumption was a compressible sea bed. This implies that the pressure response in the seabed changes drastically as a function of

the permeability of the sea bed material. Unlike Moshagen and Torum (1975), Madsen (1978) developed a theory where both fluid and soil skeleton were considered compressible. Referring to the undesirable discontinuity at the water sediment interface of the inviscid model used in early works mentioned above, McClain (1977) utilized the "radiation-type" boundary condition found in other physical problems such as heat conduction in order to understand the behavior of linear waves leaving the solution domain. Yamamoto (1978) developed a mathematical model for the behavior of the fluid/porous medium where they utilized Biot's consolidation theory. Their aim was to examine the sea bed response to the water waves as a combination of the fluid and solid mechanical effects. Puri (1978) showed that viscosity may not be the dominant influence in the damping mechanism since the damping effects due to percolation in the fixed sea bed may be of the same or even higher order than those due to viscosity. Puri (1980) presented the damping characteristics of a progressive wave over the contaminated surface of a viscous fluid, which is bounded below by a porous sea bed. The contributions of capillary and gravitational effects are investigated to the decay of the surface waves. Saks (1986) considered the problem of gravity waves over a permeable sea bed within the framework of the linear wave theory in a flow over an impermeable sea bed, from which a wave pressure function was determined and the wave motion in the porous sea bed had been treated as a secondary motion determined by the fluctuations of the wave pressure on the bottom line.

Among many numerical wave modeling studies done in the past, the list of studies that are in this study's interest, can be initiated with Liu et al. (1980) who applied Boundary Integral Equation Method (BIEM) to the transient wave problems where only two dimensional linearized waves were taken into account. For the linearized boundary conditions, the nodes were imbedded in the horizontal free surface location of the resting fluid rather than placing the nodes on the instantaneous free surface as an advantage of BIEM, which has proved it to be an efficient and accurate numerical scheme in the solution of free-surface problems. Cruz (1997) used the method of finite differences to solve the Boussinesq equations for porous sea beds which contain the leading orders of nonlinearity and dispersivity. Li and Barry (1999) developed a numerical model to examine the basic features of instantaneous and phase-averaged beach groundwater flows which are induced by waves. Their model simulates the interaction between wave motion and groundwater

flow where non-linear shallow water equation was used to describe the wave motion on the beach. A dissipative finite difference scheme based on the Lax-Wendroff conservation method is used to solve the two dimensional equations mentioned above. Lui (1999) described the flow in porous structures by the spatially averaged Navier-Stokes equations. Their model calculates the mean flow outside of porous structures based on the Reynolds Averaged Navier-Stokes (RANS) equations. Hsiao (2001) developed two-dimensional depth-integrated model equations describing nonlinear water waves propagating over a porous sea bed. In the numerical model, the third order explicit Adams-Bashforth predictor step and the fourth order implicit Adams-Moulton corrector step is adopted while the fourth order finite difference method is used for all spatial derivatives. Karunarathna and Lin (2006) developed a numerical model to study the wave damping over porous sea beds. The flow outside the porous media is described by Reynolds Averaged Navier-Stokes (RANS) equations and the spatially averaged Navier-Stokes equations are implemented for the flow inside the porous zone. Cheng (2009) introduced a coupled numerical model of wave interaction with porous medium. Two dimensional RANS equations with $k\varepsilon$ closure are used for the wave field solver and nonlinear Forchheimer equations are adopted to calculate the flow inside the porous media. The numerical method of choice in this paper is the Piecewise Linear Interface Construction - Volume of Fluid (PLIC-VOF) which is a flexible and an efficient method for treating free surface boundaries. Cheng (2012) did another study using the same set of equations and the same numerical approach for highly permeable sea beds. Compared to the results of their previous work, their results indicate that wave-induced pore water pressure has larger values and stronger action on seabed with different parameters. Another simulation based on the numerical solution of Navier-Stokes equations was presented by Dimas and Kolokythas (2011). In their approach, the equations were transformed so that the computational domain became time-independent. As their numerical method, they have adopted a hybrid scheme for the spatial discretization with finite differences in the stream wise direction and a pseudo spectral approximation with Chebyshev polynomials in the vertical direction. Kim and Lee (2012) developed a theoretical model based on the Eigen function expansion method to simulate the propagation of waves over a porous sea bed. Pudjaprasetya and Magdalena (2013) studied the effectiveness of a submerged permeable breakwater with the Lax-Wendroff method which is a finite difference method. Wang (2012) developed an improved collocation meshless method based on the variable shaped RBF for the solution of the interior acoustic

problems. Wang and Chen (2013) studied the seepage under cnoidal waves using the transient seepage equation. Silva (2002) derived time-independent mild slope equations (MSE) for waves on a finite porous bed. The numerical approach in their paper is the centered finite-difference method. Silva (2003) used an extended version of the set of equations mentioned above for waves travelling over a rapidly changing porous bottom. Silva (2005) presented a numerical solver for the modified time-independent mild slope equation which incorporates energy dissipation. The steady-state modified mild slope equation is solved by using a finite difference scheme together with a second-order parabolic approximation. Silva (2006), again using the modified time independent mild-slope equation for linear waves over a rapidly changing finite porous sea bed, presented a numerical model in which the reflection and phase coefficient shift are solved implicitly. The numerical methods used in this paper are the same as previously mentioned above.

As mentioned before, an important part of this study is the numerical modeling of flows inside a sandy sea bed. Some of the previous studies summarized above includes the porous media, either as permeable breakwater or as permeable sea bed, in their formulations and calculations. However, the literature material which include porous structures above, commonly focus on how wave passing over these structures attenuate. The literature material which deals with the flows inside the porous bed and the transportation processes that are in the scope of this study starts with Shum (1992) who examined the exchange between the water column and the sea bed and the wave-induced advective transport below a rippled sea bed. In his study, he concluded that the total exchange across the water-seabed interface, averaged over one wave period, is significantly higher across a rippled interface than across a flat seabed. Also, it is pointed out that this difference increases with increasing ripple slope and the strength of the wave motion and it decreases with increasing thickness of sediment layer relative to the length of the gravity wave. Shum (1993) investigated the effects of wave-induced pore water circulation on the transport of reactive solutes below a rippled sediment bed. Significant spatial variations were found where the concentration below a ripple trough can be many times higher than that at the same depth below a crest, and the concentration gradient in the horizontal can be of the same order of magnitude as that in the vertical. To investigate the characteristics of wave motion within homogenous, undeformable porous media under a rippled sea bed, Zhu (2000) developed an approach by applying Sollitt and Cross' (1972)

method and the Galerkin Eigen function expansions to derive a modified linear refraction-diffraction model of water waves inside a porous medium. The numerical method used in this paper is the finite difference method. Massel (2001) presented a theoretical attempt to predict the groundwater circulation due to wave set-up. Two systems of circulations have been discovered, related to two different gradients of the set-up height. For the offshore gradient, the horizontal excess pressure gradient induces flow in the offshore direction while, closer to the shore, the pressure gradient is reversed and the resulting flow moves shoreward. Ting (2004), investigated how the porosity of submerged breakwaters affects non-breaking wave transformations. In their experiments, the porosity varied from 0.421 to 0.912 so that various porosities with different breakwater geometries are studied to gather more information about porosity effects on wave fields. Tsai (2005), in their study of wave transformation over submerged permeable breakwater on porous bottom, derived the time-independent mild slope equation for waves propagating over two layers of porous medium. The numerical approach in their paper is a finite-difference scheme with staggered meshes and mid-time grids.

Some of the literature material includes experimental studies which are helpful while checking the correctness of the results at hand. Corvaro (2010) performed laboratory experiments to study the wave damping induced by a porous seabed. They have observed decay in a significant decay in wave height and an increase in wavelength. They have also studied the influence of the geometric properties of the porous bed on the wave dissipation. They found that as the thickness of porous bed increases, the attenuation of the wave height also increases. Another paper that includes experimental data belongs to De Drezigue (2013) where they have investigated the wave propagation over a rectangular porous bar and their results indicate that the interference process is weakly influenced by the porosity of the bar and by the presence of impervious vertical boundaries at both sides of the bar.

The most inspiring papers for this thesis study are Wu, Tsay and Young (2005) and Wu, Tsay and Young (2008) in which the authors use boundary-only-type radial basis collocation method (RBFCM) for solving nonlinear free surface water waves. In the boundary-only meshless method, the fundamental solution of the linear operator can be chosen as the radial basis function (RBF) which automatically satisfy the governing equation except at the center of RBF. If RBF centers are located outside the computational

domain, emergence of a singularity problem is avoided and only few collocation points on the boundary are needed to be solved. By using the method of fundamental solutions (MFS), the only task is to satisfy boundary conditions since the governing equation is satisfied automatically. The type of RBF that they used in their study is the fundamental solution of a two dimensional Laplace equation; $f_{ij} = \ln r_{ij}$. In their latter paper, Wu, Tsay and Young (2008), the Gaussian function is chosen to be the RBF so that they can increase the accuracy of the derivative term computations on the free surface. In order to avoid singularity problems, they use different locations for RBF centers and collocation nodes.

3. WAVE PROPAGATION: THE BOUNDARY VALUE PROBLEM

3.1. Wave Propagation over a Horizontal and Impervious Sea Bed

The boundary value problems and their analytical solutions for wave propagation over horizontal and impervious/pervious sea beds are presented in this chapter. The boundary value problems are used to constitute numerical models and their analytical solutions are utilized to investigate and to verify numerical models` ability of simulating the physical phenomenon.

The boundary value problem for two-dimensional linear waves propagating over a horizontal and impervious sea bed is summarized as (the wave motion is simple harmonic with angular frequency ω);

$$\begin{aligned} &\nabla^2\phi = 0; && -h < z < 0 \\ &\phi_z + \eta_t = 0; && z = 0 \\ &\phi_t + g\eta = 0; && z = 0 \\ &\phi_z = 0; && z = -h \end{aligned} \tag{3.1}$$

In the set of equations given in (3.1), the first equation is the governing equation (the Laplace equation), the second equation is the kinematic free surface boundary condition (KFSBC), the third equation is the dynamic free surface boundary condition (DFSBC) and the last equation is the bottom boundary condition (BBC).

The combined free surface boundary condition can be formed by multiplying the KFSBC by g and subtracting, from the result, the time derivative of the DFSBC which can be used as a free surface boundary condition just like the KFSBC and the DFSBC,

$$\phi_{tt} + g\phi_z = 0; \qquad z = 0 \tag{3.2}$$

To obtain wave solutions which are both periodic with T and wavelength L, let,

$$\phi = \mathrm{Re}\left[\varphi(x,z)e^{-i\omega t}\right] \tag{3.3}$$

$$\eta = \mathrm{Re}\left[\xi(x)e^{-i\omega t}\right] \tag{3.4}$$

Here, $\omega = 2\pi / T$ is the angular frequency and φ, ξ are the complex amplitudes of ϕ and η. When using Equations (3.3) and (3.4), writing $\mathrm{Re}[\ ]$ will be omitted until results are obtained. Using Equation (3.3) and Equation (3.4) in Eq. 3.1,

$$\begin{aligned} &\varphi_{xx} + \varphi_{zz} = 0; && -h < z < 0 \\ &\varphi_z - i\omega\xi = 0; && z = 0 \\ &i\omega\varphi + g\xi = 0; && z = 0 \\ &\varphi_z = 0; && z = -h \end{aligned} \tag{3.5}$$

Attempting a separation of variable solution of the Laplace equation, let,

$$\varphi(x,z) = X(x)Z(z) \tag{3.6}$$

so that,

$$\frac{dX(x)}{dx^2} + \frac{dZ(z)}{dz^2} = 0 \tag{3.7}$$

Equation (3.7) can be satisfied only if,

$$\frac{d^2X(x)}{dx^2} = -\frac{d^2Z(z)}{dz^2} = c \tag{3.8}$$

where c is a constant. Depending on whether c is negative, positive or zero, different solutions are obtained to the governing equation. Investigating all cases to choose the appropriate one,

Case 1. $c > 0$;

$X \propto \begin{cases} e^{-\sqrt{c}x} \\ e^{+\sqrt{c}x} \end{cases} \rightarrow$ No good since X is not periodic and is unbounded or dies out as $x \rightarrow \pm\infty$.

$Z \propto \begin{cases} \cos\sqrt{c}z \\ \sin\sqrt{c}z \end{cases} \rightarrow$ No good since Z does not die out with depth.

Case 2. $c = 0$,

$X = Ax + B \rightarrow$ No good since solution is not periodic and is unbounded as $x \rightarrow \pm\infty$.

$Z = Cz + D$

For the X solution, we could set A to zero. This would mean that B should be a constant. However; if B is other than zero, we have the entire sea surface rising and falling at the same time which violates continuity.

Case 3. $c = -k^2 < 0$,

$$X \propto \begin{cases} e^{ikx} \\ e^{-ikx} \end{cases}$$

$$Z \propto \begin{cases} e^{kz} \\ e^{-kz} \end{cases}$$

The X solution is periodic in horizontal plane. Since the solution needs to be periodic with the wave length,

$$k = \frac{2\pi}{L} \tag{3.9}$$

The solution so far is,

$$\phi = (Ae^{ikx} + Be^{-ikx})(Ce^{-kz} + De^{kz})e^{-i\omega t} \tag{3.10}$$

Using ϕ in the CFSBC and the BBC yields,

$$\begin{aligned} &(-i\omega)^2\varphi + g\varphi_z = 0 && z = 0 \\ &\varphi_z = 0 && z = -h \end{aligned} \tag{3.11}$$

or,

$$\begin{aligned} &C\left(-1-\frac{\omega^2}{gk}\right) + D\left(1-\frac{\omega^2}{gk}\right) = 0 \\ &C(-e^{kh}) + D(e^{-kh}) = 0 \end{aligned} \tag{3.12}$$

The set of equations can be written in matrix for as,

$$\begin{pmatrix} -1-\frac{\omega^2}{gk} & 1-\frac{\omega^2}{gk} \\ -e^{kh} & e^{-kh} \end{pmatrix} \begin{Bmatrix} C \\ D \end{Bmatrix} = \begin{Bmatrix} 0 \\ 0 \end{Bmatrix} \tag{3.13}$$

For non-trivial solutions, the determinant of the coefficient matrix should vanish. This leads to the equation,

$$-\frac{\omega^2}{gk}\left[e^{kh}+e^{-kh}\right]+\left[e^{kh}-e^{-kh}\right]=0$$
$$-\frac{\omega^2}{gk}\cosh kh+\sinh kh=0 \tag{3.14}$$
$$\boxed{\omega^2=gk\tanh kh}$$

Equation (3.14) is the wave dispersion equation which is the solvability condition of the system of equations formed by the CFSBC and the BBC.

To continue with the solution, returning to the BBC,

$$-Ce^{kh}+De^{-kh}=0\rightarrow D=Ce^{2kh} \tag{3.15}$$

$Z(z)$ becomes,

$$Z(z)=Ce^{-kz}+De^{kz}=C(e^{-kz}+e^{2kh}e^{kz})=Ce^{kh}(e^{-k(z+h)}+e^{k(z+h)})$$
$$Z(z)=C'\cosh k(z+h) \tag{3.16}$$

C' is another constant. Summarizing the solution so far,

$$\phi=(Ae^{ikx}+Be^{-ikx})\cosh k(h+z)e^{-i\omega t}$$
$$=(Ae^{i(kx-\omega t)}+Be^{-i(kx-\omega t)})\cosh k(h+z) \tag{3.17}$$

C' has been absorbed into A and B. The solution above indicates a standing wave which is the superposition of a left going wave and a right going wave. That is,

$$kx-\omega t\Rightarrow right\ \ going\ \ wave$$
$$kx+\omega t\Rightarrow left\ \ going\ \ wave \tag{3.18}$$

Supposing that right going progressive waves are in the scope, $B=0$ so that,

$$\phi=A\cosh k(h+z)e^{i(kx-\omega t)} \tag{3.19}$$

From the DFSBC,

$$\eta=\frac{1}{g}\phi_t\Big|_{z=0}=-\frac{i\omega}{g}A\cosh kh\,e^{i(kx-\omega t)} \tag{3.20}$$

Taking the right going progressive wave to be a cosine wave with real amplitude a, A is determined as,

$$\eta = ae^{i(kx-\omega t)} = -\frac{i\omega}{g} A\cosh kh\, e^{i(kx-\omega t)} \Rightarrow A = i\frac{ag}{\omega}\frac{1}{\cosh kh} \tag{3.21}$$

The velocity potential and the free surface displacement becomes,

$$\begin{aligned} \phi &= \mathrm{Re}\left[i\frac{ag}{\omega}\frac{\cosh k(h+z)}{\cosh kh} e^{i(kx-\omega t)} \right] \\ \phi &= -\frac{ag}{\omega}\frac{\cosh k(h+z)}{\cosh kh}\sin(kx-\omega t) \end{aligned} \tag{3.22}$$

$$\begin{aligned} \eta &= \mathrm{Re}\left[ae^{i(kx-\omega t)} \right] \\ \eta &= a\cos(kx-\omega t) \end{aligned} \tag{3.23}$$

3.2. Wave Propagation over a Horizontal and Pervious Sea Bed

To set up the boundary value problem and to obtain analytical expressions for the velocity potentials and the free surface displacement for waves propagating over a pervious sea bed, two assumptions are made;

(i) Waves propagating over the permeable sea bed are linear and progressive.

(ii) Flow inside the sand layer is governed by Darcy's Law.

$$\psi = \frac{P}{\rho g} + z \rightarrow \text{Pressure head + Elevation head} \tag{3.24}$$

$$\vec{U}_s = (u_s, w_s) = -K\nabla\psi \tag{3.25}$$

where K is the permeability coefficient of the sea bed and (u_s, w_s) are the velocity components inside the porous media. The flow in the sand layer must satisfy the continuity equation for incompressible flow, thus it is governed by the Laplacian equation.

It is further assumed that the flow inside the sea bed is in phase with the wave motion and the flow inside the sea bed responds without lag to the dynamic pressure from the wave motion.

Boundary conditions for the permeable sea bed case are; there is no flow through the impermeable layer under the permeable zone at $z=-(h+h_d)$ (h is water depth and h_d is sand layer thickness). At the interface between the sea zone and the permeable sea bed zone, there are pressure match and vertical velocity match conditions, both stating that velocity and pressure values are in phase. Finally, at the free surface, combined free surface boundary condition exists. To sum up the boundary value problem;

$$\begin{aligned}
&\nabla^2\phi = 0 && (-h \le z \le 0)\\
&\phi_{tt} + g\phi_z = 0 && (z=0)\\
&\phi_z + K\psi_z = 0 && (z=-h)\\
&\psi + \frac{1}{g}\phi_t = 0 && (z=-h)\\
&\nabla^2\psi = 0 && (-h-h_d \le z \le -h)\\
&\psi_z = 0 && (z=-h-h_d)
\end{aligned} \tag{3.26}$$

Governing equations for flow inside and above sand layer are linear so expressions for velocity potentials inside and above the permeable sea bed can be assumed as;

$$\phi = \varphi(z)e^{-i(kx-wt)} \tag{3.27}$$

$$\psi = \hat{\psi}(z)e^{-i(kx-wt)} \tag{3.28}$$

Using Equation (3.27) and Equation (3.28) in Equation (3.26);

$$\begin{aligned}
&\varphi_{zz} - K^2\varphi = 0 && (-h \le z \le 0)\\
&\varphi - \frac{\omega^2}{g}\varphi_z = 0 && (z=0)\\
&\varphi_z + K\hat{\psi}_z = 0 && (z=-h)\\
&\hat{\psi} + i\frac{\omega}{g}\varphi = 0 && (z=-h)\\
&\hat{\psi}_{zz} - K^2\hat{\psi} = 0 && (-h-h_d \le z \le -h)\\
&\hat{\psi}_z = 0 && (z=-h-h_d)
\end{aligned} \tag{3.29}$$

For the solutions of the second and the sixth equations, Equation (3.29),

$$\varphi = a_1\cosh k(h+z) + b_1\sinh k(h+z) \tag{3.30}$$

$$\hat{\psi} = a_2\cosh k(h_d+h+z) + b_2\sinh k(h_d+h+z) \tag{3.31}$$

Using Eq. 3.31 in the sixth equation of Equation (3.29) (taking the real part of (3.31), $b_2 = 0$);

$$\hat{\psi} = a_2 \cosh k(h_d + h + z) \tag{3.32}$$

Using Eq. 3.30 in the second equation of Equation (3.29);

$$a_1\left(\tanh kh - \omega^2 / gk\right) + b_1\left(1 - \left(\omega^2 / gk\right)\tanh kh\right) = 0 \tag{3.33}$$

Using Eq. 3.30 and Eq. 3.31 in the third equation of Equation (3.29);

$$b_1 + a_2 K \sinh kh = 0 \tag{3.34}$$

Using Eq. 3.30 and Eq. 3.31 in the fourth equation of Equation (3.29);

$$a_2 \cosh kh_d + i\frac{\omega}{g}a_1 = 0 \tag{3.35}$$

Equation (3.33), Equation (3.34) and Equation (3.35) constitute a set of equations in terms of the unknowns a_1, a_2 and b_1. For simultaneous non-trivial solution to exist the determinant of the coefficient matrix should vanish.

$$\begin{pmatrix} \tanh kh - \omega^2 / gk & 1 - \left(\omega^2 / gk\right)\tanh kh & 0 \\ 0 & 1 & K \tanh kh \\ i\dfrac{\omega}{g} & 0 & 1 \end{pmatrix}$$

Expanding and rearranging,

$$\frac{\omega^2}{gk \tanh kh} = 1 + i\frac{\omega K}{g}\tanh kh\left(\coth kh - \frac{\omega^2}{gk}\right) \tag{3.36}$$

The equation above is the dispersion relation for waves passing over a pervious sea bed. It should be noted that, the dispersion relation for waves over an impervious bottom may be recovered by setting $K = 0$ in Equation (3.36).

Summarizing φ and $\hat{\psi}$;

$$\varphi = \left(a_1 \cosh k(h + z) + b_1 \sinh k(h + z)\right)e^{-i(kx - \omega t)} \tag{3.37}$$

$$\hat{\psi} = \left(a_2 \cosh k(h_d + h + z)\right)e^{-i(kx - \omega t)} \tag{3.38}$$

Considering a surface disturbance of the form;

$$\eta = A_0 e^{i(kx-\omega t)} \tag{3.39}$$

Using Equation (3.37) in kinematic free surface boundary condition;

$$\eta = -\frac{1}{g}\varphi_t \tag{3.40}$$

For the maximum value of η it yields;

$$-i\frac{\omega}{g}\left(a_1 \cosh kh + b_1 \sinh kh\right) = a \tag{3.41}$$

a_1 and b_1 may be solved in terms of a_2 from Equation (3.34) and Equation (3.35);

$$a_1 = -\left(\frac{1}{i\omega g}\right) a_2 \cosh kh_d \tag{3.42}$$

$$b_1 = -a_2 K \sinh kh_d \tag{3.43}$$

Using Equation (3.42) and Equation (3.43) in Equation (3.41);

$$a_2 = \frac{a}{\cosh kh_d \cosh kh\left(1 + i\frac{\omega K}{g}\tanh kh \tanh kh_d\right)} \tag{3.44}$$

or letting;

$$C = 1 + i\omega\frac{K}{g}\tanh kh \tanh kh_d \tag{3.45}$$

$$a_2 = \frac{a}{C \cosh kh_d \cosh kh} \tag{3.46}$$

Using Equation (3.45) in Equation (3.44) and Equation (3.43);

$$a_1 = i\frac{g}{\omega}\frac{a}{C \cosh kh} \tag{3.47}$$

$$b_1 = -a\frac{K \tanh kh_d}{C \cosh kh} \tag{3.48}$$

Using Equation (3.46) to Equation (3.48) to rewrite Equation (3.30) and Equation (3.31), we derive expressions for the velocity potentials in the sea and in the sand zone;

$$\varphi = i\frac{ag}{\omega}\left(\frac{1}{C}\right)\left(\frac{\cosh k(h+z)}{\cosh kh} + i\frac{\omega K}{g}\tanh kh_d \frac{\sinh k(h+z)}{\cosh kh}\right)e^{-i(kx-\omega t)} \tag{3.49}$$

$$\psi = \frac{a}{C\cosh kh\cosh kh}\cosh k(h_d + h + z)e^{-i(kx-\omega t)} \tag{3.50}$$

4. NUMERICAL METHODS AND MODELING

4.1. Meshless Methods

Meshless methods are numerical simulation methods that do not require formation of a mesh neither inside the solution domain nor on the solution domain boundaries. Previous numerical simulation methods such as finite difference method, finite volume methods and finite element method are defined on meshes of data points on the solution domain in which each data point has a fixed number of predefined neighboring points. These neighboring points are used to define mathematical operators such as a derivative and then, by using these mathematical operators, the equations are constructed and defined. However, while simulating a physical phenomenon in which the material is moving or where large deformations of the material can occur, linkage between data points by meshes can be difficult to maintain without involvement of an error. Wu et. al (2006) addresses this difficulty by stating the following: "For traditional numerical methods (such as FEM or FDM for example), non-fixed (deforming) meshes are needed. Usually, an excess number nodes and a huge size of matrix accompany with the formulation if one tries to solve the problem by conventional numerical methods." Meshless methods, on the contrary, require no formation of mesh, they make use of a set of nodes placed inside the solution domain and on its boundaries which makes them more flexible while handling problems with moving boundaries or problems with large deformations. In literature, there are several techniques to fix these, yet, none are as effective as meshless methods which are intended to remedy these problems.

In recent decades, meshless methods are becoming more and more popular among the scientists and the engineers who are in search of more efficient numerical techniques in terms of computing time and programming effort. Several meshless methods have been proposed over the last decade, these are namely, Smoothed Particle Hydrodynamics (SPH), Diffuse Element Method (DEM), Meshless Local Petrov-Galerkin Method (MLPG) and Radial Basis Function Collocation Method (RBFCM). In this study, the Radial Basis Function Collocation Method is utilized to solve the boundary value problem at hand.

4.2. Radial Basis Function Collocation Method

The Radial Basis Function Collocation Method (RBFCM), a meshless numerical simulation method, was first introduced by Kansa (1990a, 1990b). This method can be used to solve elliptic, parabolic or hyperbolic partial differential equations. The RBFCM is based on the idea of constructing a function from the known information of the problem such as governing equations, boundary conditions and initial conditions. Two sets of points are defined inside the solution domain and on its boundaries which are called collocation nodes and radial basis function centers. At the collocation nodes, the known information about the problem (governing equations, boundary conditions, and initial conditions) are defined and at the radial basis function centers (denoted as RBF centers) are the nodes where the chosen radial basis functions are defined. Collocation nodes and RBF centers may be located at the same geometrical coordinates or they may be at totally different locations. Radial basis functions are the functions of geometrical distances between these two set of points. The mathematical theory behind RBF`s may be found in Buhmann (2003).

In order to approximate, $u(x,y,z,t)$ by using a RBF;

$$u_i = f_{ij}(r)\alpha_j(t) \qquad i, j = 1,2,...,N \tag{4.1}$$

Here, i and j are the collocation nodes and RBF centers respectively and α_j are the coefficients for the approximation, which can be functions of time. N is the total number of nodes used for approximation, f is the radial basis function and r is the distance between two nodes. The distance between two nodes is given as;

$$r=\sqrt{\left(x_i-x_j\right)^2+\left(y_i-y_j\right)^2+\left(z_i-z_j\right)^2} \tag{4.2}$$

The spatial derivatives of the function $u(x,y,z,t)$ can be obtained by differentiating (4.1);

$$\frac{\partial^n u_i}{\partial \varsigma^n} = \frac{\partial^n f_{ij}}{\partial \varsigma^n}\alpha_j \tag{4.3}$$

where ς is one of the coordinate directions. The first derivative of f_{ij} with respect to ς is;

$$\frac{\partial f_{ij}}{\partial \varsigma} = \frac{\partial f_{ij}}{\partial r}\frac{\partial r}{\partial \varsigma} = \frac{\partial f_{ij}}{\partial r}\frac{\left(\varsigma_i - \varsigma_j\right)}{r} \tag{4.4}$$

While solving a boundary value problem, the approximation and its derivatives can be used to generate a system of *N* linear algebraic equations in *N* unknowns to be solved for u . This can be summarized as;

$$\begin{aligned} Lu_i &= 0 \qquad i = 1,2,...,L \\ Bu_i &= 0 \qquad i = L+1, L+2,..., N \end{aligned} \tag{4.5}$$

Above, L operator is related to the information inside the solution domain and B is related to the information on the solution domain boundaries. Some of the commonly used radial basis functions are given in Table 4.1.

Table 4.1. Commonly used RBFs

RBF	$f(r)$
Multiquadrics(MQ)	$\left(r^2 + c^2\right)^{\beta/2} \qquad \beta > 0, \beta \in 2N+1$
Inverse Multiquadric	$\left(r^2 + c^2\right)^{-\beta/2} \qquad \beta > 0, \beta \in 2N+1$
Splines	$r^{\beta} \qquad \beta > 0, \beta \in 2N+1$
Thin Plate Splines (TPS)	$r^{\beta} \ln r \quad \beta > 0, \beta \in 2N$
Gaussian	$\exp(-c^2 r^2)$
Wendland's compactly supported	$(1-r/R)^4 + (1+4r/R)$

The utilization of RBFCM in this study enables to model different length scales without facing problems. For example, wavelength is of $\mathrm{O}(10)$ m while the ripple length at

the sea bed is of $O(0.1)$m. Classical numerical methods, which require mesh generation inside the solution domain and on solution domain boundaries, need extra programming effort and computational storage. If any other method that requires a mesh generation were to be used, the mesh size must be based on the smallest scale so that there would be no loss in resolution. The flexibility of RBFCM in node placement provides an important advantage over other numerical methods since the programming effort reduces significantly.

4.3. Boundary-Type RBFCM

According to Wu et.al (2006), there are two kinds of meshless methods: the domain-type and the boundary-type methods. In the first one, such as Kansa's method, any single RBF does not satisfy the governing equation, therefore; a large number of collocation points must be placed inside the solution domain. By doing so, neither the number of nodes nor the size of matrix is reduced so the only advantage of using domain-type meshless methods is easy programming and avoids mesh generation. However, when using the boundary-type methods for solving partial differential equations such as Laplace, Helmholtz etc., the fundamental solution of the linear operator can be chosen as RBF. By doing so, the governing equation is automatically satisfied and the remaining task is to satisfy the boundary conditions. The matrix size reduces since no collocation points are placed inside the governing equation zone and less programming effort is required and less computer storage is used. This method is also called the Method of Fundamental Solutions (MFS).

The scope of this study is the modeling of the surface waves and the induced flows inside a sandy sea bed. The governing equation for both sea domain and sand domain is the Laplace equation. The choice of the RBF is the Green's function of the Laplace equation; $f_{ij} = \ln r_{ij}$. Since the governing equation`s information is indirectly given to the model by the RBF, there is no need to place collocation nodes inside the solution domain. The problem is solved on the solution domain boundaries and then, the values obtained here are interpolated, again using the RBFCM interpolation scheme, to find the values inside the solution domain. A faster and less tedious programming effort is achieved by following

this procedure. Also here, it should be noticed that, if $r = 0$ in the RBF, which means that the collocation nodes and the RBF centers coincide, singularity problems in matrices occur. To prevent such a problem, the collocation points and the RBF centers are placed at different locations.

The boundary-type RBFCM is applied to the wave propagation boundary value problems which have been explained in the previous chapter. Firstly, wave propagation over an impervious sea bed problem has been taken into account and an algorithm for solving the BVP has been prepared. At this stage, it has been verified that the boundary-type RBFCM can be an effective method for the problems at hand. Next, an algorithm for wave propagation over pervious sea bed has been prepared. Detailed explanations of these algorithms are given in the following sections.

4.4. Boundary-Type RBFCM for Wave Propagation over an Impervious Sea Bed

The first step of the present study is the application of the boundary-type RBFCM to a wave propagation problem over an impervious sea bed. An algorithm for solving the problem at hand has been created. This section covers the details of the first algorithm created by using boundary-type RBFCM. As stated in the previous section, the RBF, $f_{ij} = \ln r_{ij}$, is weakly singular to start with, the derivatives of the RBF will also be singular. To avoid singularity, different sets of nodes are used for the collocation points and the RBF centers as shown in the figure (4.1). The solution domain extends from the still water level at $z = 0\,\text{m}$ to the impervious bottom at $z = -2\,\text{m}$.

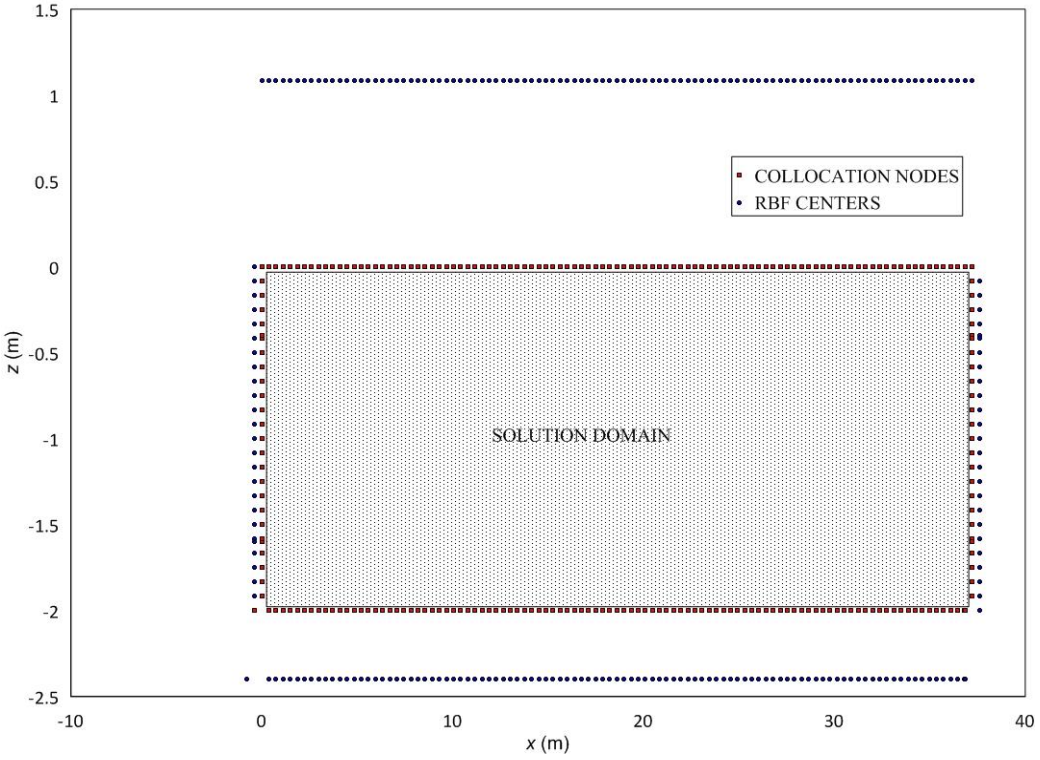

Figure 4.1. The node placement scheme for the linear wave propagation problem.

Since the collocation nodes and the RBF centers are different set of nodes, the geometric distane between collocation nodes and the RBF centers is defined as ;

$$r_{ij} = \sqrt{\left(x_i^{\,c} - x_i^{\,r}\right)^2 + \left(y_i^{\,c} - y_i^{\,r}\right)^2} \tag{4.6}$$

where the superscripts c and r stand for the collocation nodes and the RBF centers, respectively. The first derivatives of the RBF are defined may be defined as;

$$f_{ij}^{\,x} = \frac{\left(x_i^{\,c} - x_i^{\,r}\right)}{r_{ij}^{\,2}} \qquad f_{ij}^{\,y} = \frac{\left(y_i^{\,c} - y_i^{\,r}\right)}{r_{ij}^{\,2}} \tag{4.7}$$

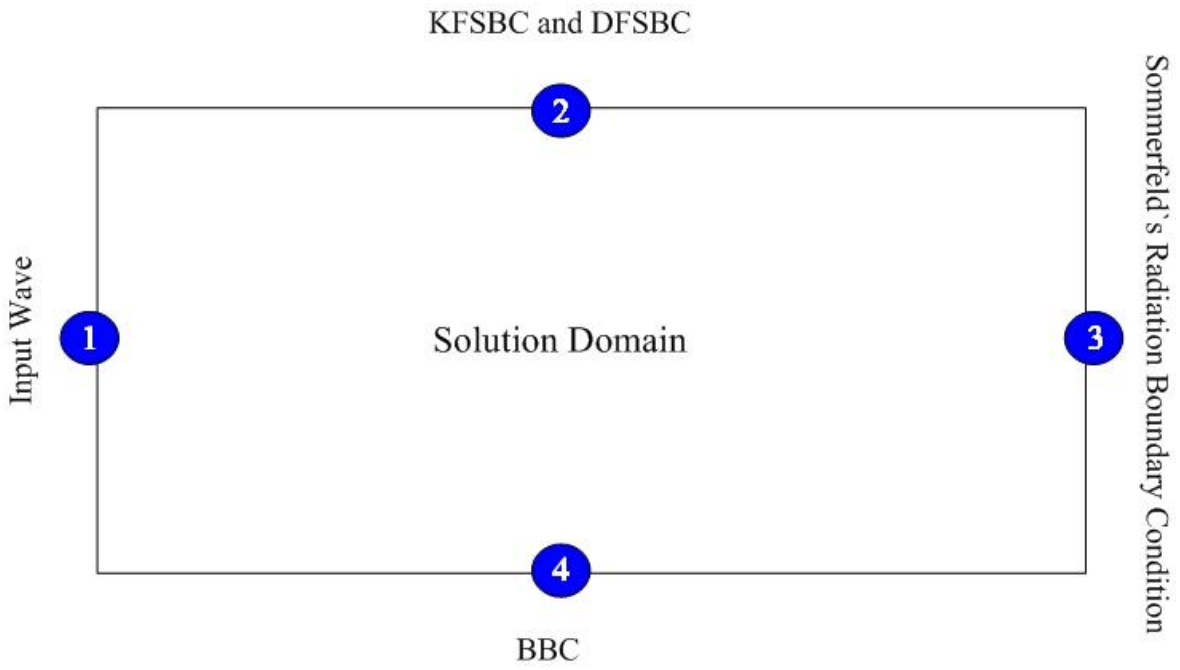

Figure 4.2. Summary of the BVP.

The boundary value problem for wave propagation is presented in the figure below where a single collocation point is shown on each surface of the solution domain. On the left vertical face of the solution domain the incident linear wave is specified. On the right vertical face of the solution domain Sommerfeld's radiation boundary condition (RBC) is used. The top surface has the kinematic free surface boundary condition and the dynamic free surface boundary condition. On the bottom of the solution domain, the vertical component of the velocity is defined as zero.

The proposed procedure to advance the solution from time level n to $n+1$,

(i) Update the wave input $\varphi_1^{(n+1)} = \varphi_1^{*(n+1)}$.

(ii) Integrate the KFSBC and the DFSBC for $\varphi_2^{(n+1)}, \eta_2^{(n+1)}$. $\varphi_2^{(n+1)}$ to be used as Dirichlet type information $\varphi_2^{*(n+1)}$.

(iii) Integrate Sommerfeld`s radiation boundary condition for $\varphi_3^{(n+1)}$. $\varphi_3^{(n+1)}$ to be used as Dirichlet type information $\varphi_3^{*(n+1)}$.

(iv) Update the right hand side vector b using the results of steps 1, 2 and 3.

(v) Determine $\varphi^{(n+1)} = S^{-1}b^{(n+1)}$.(where S is the system matrix)

(vi) Restore Dirichlet conditions. ($\varphi_1^{(n+1)}, \varphi_2^{(n+1)}, \varphi_3^{(n+1)}$)

(vii) Determine the derivatives $\varphi^{x(n+1)}$ and $\varphi^{z(n+1)}$.

(viii) Down shift the solutions in time to prepare for the next time step. Go back to first step.

$$\begin{aligned}\eta^{(n+1)} &\to \eta^{(n)}\\ \eta^{(n)} &\to \eta^{(n-1)}\\ \eta^{(n-1)} &\to \eta^{(n-2)}\\ \eta^{(n-2)} &\to \eta^{(n-3)}\end{aligned} \tag{4.8}$$

$$\begin{aligned}\varphi_1^{(n+1)} &\to \varphi_1^{(n)}\\ \varphi_1^{(n)} &\to \varphi_1^{(n-1)}\\ \varphi_1^{(n-1)} &\to \varphi_1^{(n-2)}\\ \varphi_1^{(n-2)} &\to \varphi_1^{(n-3)}\end{aligned} \tag{4.9}$$

$$\begin{aligned}\varphi_2^{(n+1)} &\to \varphi_2^{(n)}\\ \varphi_2^{(n)} &\to \varphi_2^{(n-1)}\\ \varphi_2^{(n-1)} &\to \varphi_2^{(n-2)}\\ \varphi_2^{(n-2)} &\to \varphi_2^{(n-3)}\end{aligned} \tag{4.10}$$

$$\begin{aligned}\varphi_3^{(n+1)} &\to \varphi_3^{(n)}\\ \varphi_3^{(n)} &\to \varphi_3^{(n-1)}\\ \varphi_3^{(n-1)} &\to \varphi_3^{(n-2)}\\ \varphi_3^{(n-2)} &\to \varphi_3^{(n-3)}\end{aligned} \tag{4.11}$$

The procedure used here is different from that of Wu et.al. (2006), (2008). They use the radiation boundary condition as equation type information whereas here it is integrated first and then used as Dirichlet type information.

For time integrations, the Adams-Bashforth integrator of $\mathrm{O}(4)$;

$$y^{(n+1)} = y^{(n)} + \frac{\delta t}{24}\left(55 f^{(n)} - 59 f^{(n-1)} + 37 f^{(n-2)} - 9 f^{(n-3)}\right) \tag{4.12}$$

was used.

It should be noted that Adams-Bashforth integrator of $\mathrm{O}(4)$ requires information from past time levels. Either a self-starting method can be used for solutions at n=0,–1,–2,–3 or the analytical solutions may be used. In this study, the second one is

preferred. The Adams-Moulton corrector step was initially tested but was found to contribute negligibly to the accuracy. To save computation time, it was not used in the present study.

Integrating the kinematic free surface boundary condition and dynamic free surface boundary condition;

$$\eta_2^{(n+1)} = \eta_2^{(n)} + \frac{\delta t}{24}\left(55\varphi_{2,z}{}^{(n)} - 59\varphi_{2,z}{}^{(n-1)} + 37\varphi_{2,z}{}^{(n-2)} - 9\varphi_{2,z}{}^{(n-3)}\right) \tag{4.13}$$

$$\varphi_2^{(n+1)} = \varphi_2^{(n)} + \frac{\delta t}{24}\left(55\eta^{(n)} - 59\eta^{(n-1)} + 37\eta^{(n-2)} - 9\eta^{(n-3)}\right) \tag{4.14}$$

Integrating Sommerfeld`s radiation boundary condition;

$$\varphi_3^{(n+1)} = \varphi_3^{(n)} + \frac{\delta t}{24}(-c)\left(55\varphi_{2,x}{}^{(n)} - 59\varphi_{2,x}{}^{(n-1)} + 37\varphi_{2,x}{}^{(n-2)} - 9\varphi_{2,x}{}^{(n-3)}\right) \tag{4.15}$$

To start time integration, analytical solutions for linear waves are used;

$$\begin{aligned}
\eta^{(0)} &= a\sin(kx) \\
\eta^{(-1)} &= a\sin(kx + \omega\delta t) \\
\eta^{(-2)} &= a\sin(kx + 2\omega\delta t) \\
\eta^{(-3)} &= a\sin(kx + 3\omega\delta t)
\end{aligned} \tag{4.16}$$

$$\begin{aligned}
\varphi_{,z}{}^{(0)} &= -\frac{agk}{\omega}\frac{\sinh k(h+z)}{\cosh kh}\cos(kx) \\
\varphi_{,z}{}^{(-1)} &= -\frac{agk}{\omega}\frac{\sinh k(h+z)}{\cosh kh}\cos(kx + \omega\delta t) \\
\varphi_{,z}{}^{(-2)} &= -\frac{agk}{\omega}\frac{\sinh k(h+z)}{\cosh kh}\cos(kx + 2\omega\delta t) \\
\varphi_{,z}{}^{(-3)} &= -\frac{agk}{\omega}\frac{\sinh k(h+z)}{\cosh kh}\cos(kx + 3\omega\delta t)
\end{aligned} \tag{4.17}$$

$$\begin{aligned}
\varphi_{,x}{}^{(0)} &= -\frac{agk}{\omega}\frac{\cosh k(h+z)}{\cosh kh}\sin(kx) \\
\varphi_{,x}{}^{(-1)} &= -\frac{agk}{\omega}\frac{\cosh k(h+z)}{\cosh kh}\sin(kx + \omega\delta t) \\
\varphi_{,x}{}^{(-2)} &= -\frac{agk}{\omega}\frac{\cosh k(h+z)}{\cosh kh}\sin(kx + 2\omega\delta t) \\
\varphi_{,x}{}^{(-3)} &= -\frac{agk}{\omega}\frac{\cosh k(h+z)}{\cosh kh}\sin(kx + 3\omega\delta t)
\end{aligned} \tag{4.18}$$

Let $\varphi_i = f_{ij}\alpha_j$. Now, on the bottom boundary of the solution domain;

$$\varphi_4^{(n+1)} = 0 \rightarrow \underbrace{\left(f_{ij}^{z(n+1)}\right) f_{jk}^{-1}}_{= M_{ik}^{(n+1)}} \varphi_k^{(n+1)} = 0 \tag{4.19}$$

Now the system of equations is set and the boundary value problem in matrix form becomes;

$$\underbrace{\begin{bmatrix} 1 & 0 & 0 & 0 \\ 0 & 1 & 0 & 0 \\ 0 & 0 & 1 & 0 \\ M_{31} & M_{32} & M_{33} & M_{34} \end{bmatrix}}_{= S} \begin{Bmatrix} \varphi_1^{(n+1)} \\ \varphi_2^{(n+1)} \\ \varphi_3^{(n+1)} \\ \varphi_4^{(n+1)} \end{Bmatrix} = \begin{Bmatrix} \varphi_1^{*(n+1)} \\ \varphi_2^{*(n+1)} \\ 0 \\ \varphi_4^{*(n+1)} \end{Bmatrix} \tag{4.20}$$

Here it should also be noticed that the system matrix S is not time dependent, therefore it needs to be formed and inverted only once. On the other hand, the right-hand side vector b should be updated as time is advanced.

Once the solution which consists of all velocity potentials φ_i on the boundary has been determined, it is possible to make use of RBF interpolation to compute the velocity potentials φ_k at collocation points (x_k^c, z_k^c) inside the solution domain. To approximate the solution obtained on the boundary we have

$$\varphi_i = f_{ij}\alpha_j, \qquad i, j = 1, \ldots, N \tag{4.21}$$

The coefficients of the approximation are obtained as

$$\alpha_i = f_{ij}^{-1}\varphi_j \tag{4.22}$$

The distance between any RBF center and the collocation point (x_k^c, z_k^c) is

$$r_{kj} = \sqrt{\left(x_k^c - x_j^r\right)^2 + \left(z_k^c - z_j^r\right)^2} \tag{4.23}$$

In terms of Equation (4.23), the RBF is now redefined as

$$f_{kj} = \ln r_{kj} \tag{4.24}$$

Making use of the coefficients determined from Equation (4.22) and RBF given in Equation (4.23), the velocity potential at chosen *M* internal points can be determined from

$$\varphi_k = \sum_{j=1}^{N} f_{kj}\alpha_j, \qquad k = 1,\ldots,M \tag{4.25}$$

Since the determination of the velocity potentials at internal points only involves a series summation of N terms, it is very efficient in comparison to a domain type solution which involves matrix inversion and multiplication operations on matrices of size $(M+N)\times(M+N)$.

The accuracy of the interpolated internal point potentials can be ascertained by comparing them to the linear wave theory velocity potentials.

4.5. Boundary-Type RBFCM for Wave Propagation over a Pervious Sea Bed

The general procedure used in modeling wave propagation over an impervious sea bed, is used in the second part of the modeling effort. However, the formulation of the boundary value problem is modified according to the inclusion of a pervious sea bed of a given thickness. The geometry of the problem becomes different and, thus, the node placement scheme changes. At the sea-sand interface, two sets of RBF centers are placed because there are two matching conditions at the interface, namely the pressure match condition and the velocity match condition. The collocation nodes and the RBF centers are again defined as different set of points to avoid singularity problems. Figure 4.3 shows the node placement for wave propagation model over a pervious sea bed.

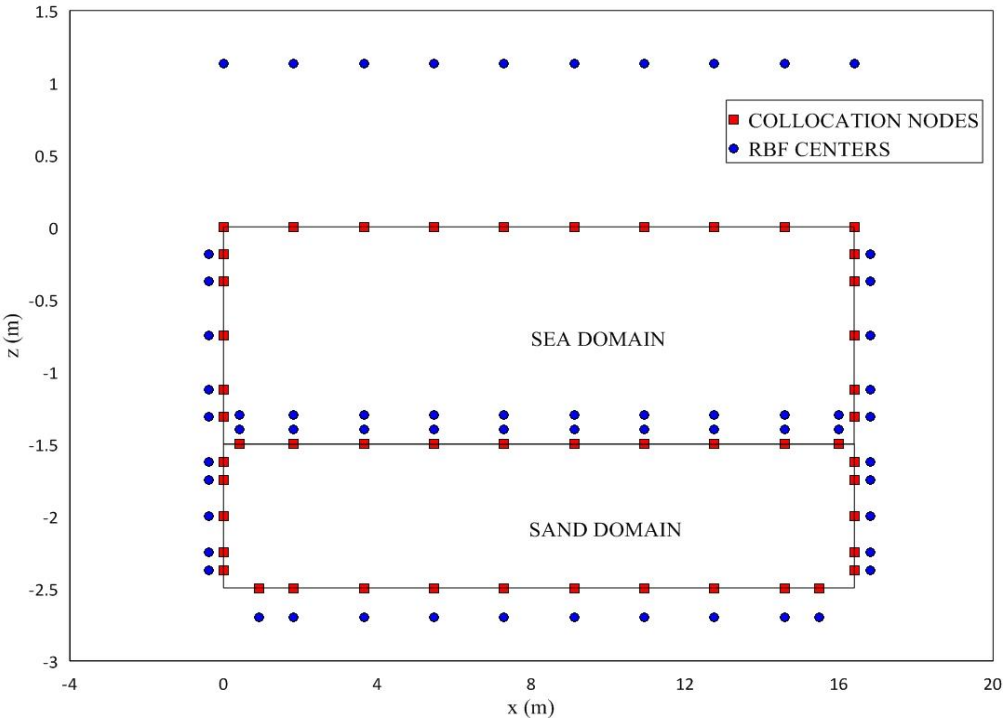

Figure 4.3. Node placement scheme for horizontal and pervious sea bed.

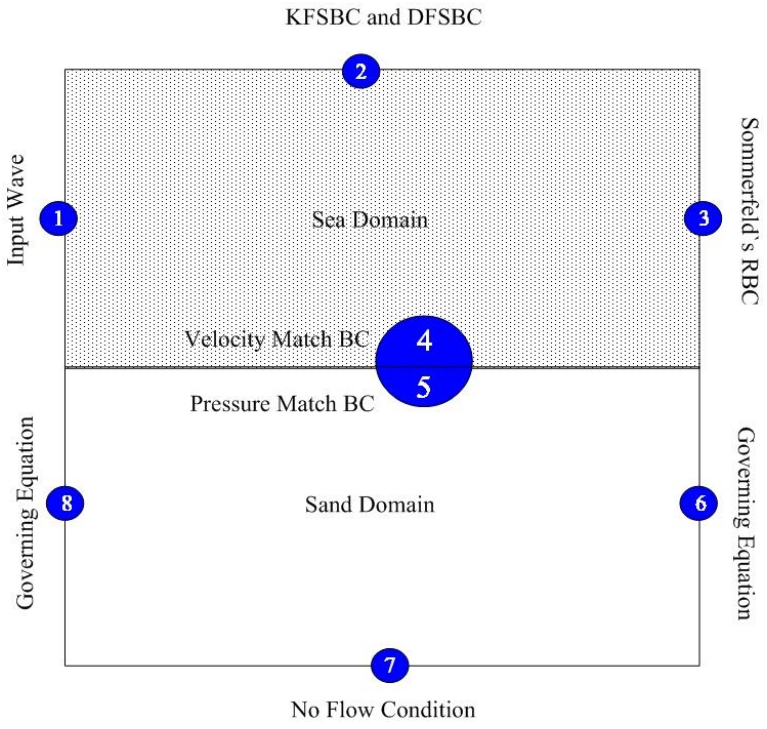

Figure 4.4. Summary of the BVP.

The boundary value problem for wave propagation is presented in the figure below where a single collocation point is shown on each surface of the solution domain. On the left vertical face of the solution domain the incident linear wave is specified. On the right vertical face of the solution domain Sommerfeld's radiation boundary condition (RBC) is used. The top surface has the kinematic free surface boundary condition and the dynamic free surface boundary condition. At sea-sand interface, the velocity match boundary condition and the pressure match boundary condition are defined. On the left and right vertical faces of the sand domain, governing equation is defined. Due to the lack of information on the lateral boundary condition for the sand domain in the literature, the Laplace equation is used at the vertical faces of the sand domain which holds for all points inside the solution domain. At the bottom of the sand domain, no flow condition is defined.

To begin formulating the BVP according to the boundary-type RBFCM, let;

$$\begin{aligned} \varphi_i &= f_{ij}\alpha_j \rightarrow \alpha_i = f_{ij}^{-1}\varphi_j \\ \psi_i &= f_{ij}\beta_j \rightarrow \beta_i = f_{ij}^{-1}\psi_j \end{aligned} \tag{4.26}$$

The first derivatives with respect to z become;

$$\begin{aligned} \frac{\partial \varphi_i}{\partial z} &= f_{ij}\alpha_j = f_{ij}^{z} f_{jk}^{-1}\varphi_k \\ \frac{\partial \psi_i}{\partial z} &= f_{ij}\beta_j = f_{ij}^{z} f_{jk}^{-1}\psi_k \end{aligned} \tag{4.27}$$

The input wave is formulated as;

$$\varphi_j^{n+1} = \varphi_j^{*n+1} \tag{4.28}$$

where " $*$ " stands for an input wave entering the solution domain.

On the free surface, the kinematic free surface boundary condition is;

$$\eta_{(i)}^{(n+1)} = \varphi_i^{(n)} + \frac{\delta t}{24} f_{ij}^{z} f_{jk}^{-1}\left(55\varphi_{(k)}^{(n)} - 59\varphi_{(k)}^{(n-1)} + 37\varphi_{(k)}^{(n-2)} - 9\varphi_{(k)}^{(n-3)}\right) \tag{4.29}$$

The dynamic free surface boundary condition is;

$$\varphi_i^{(n+1)} = \varphi_i^{(n)} - g\frac{\delta t}{24}\left(55\eta_{(i)}^{(n)} - 59\eta_{(i)}^{(n-1)} + 37\eta_{(i)}^{(n-2)} - 9\eta_{(i)}^{(n-3)}\right) \tag{4.30}$$

Sommerfeld`s radiation boundary condition is;

$$\varphi_i^{(n+1)} = \varphi_i^{(n)} - \left(\frac{c\delta t}{24}\right) f_{ij}^{\ x} f_{jk}^{\ -1} \left(55\varphi_{(k)}^{\ (n)} - 59\varphi_{(k)}^{\ (n-1)} + 37\varphi_{(k)}^{\ (n-2)} - 9\varphi_{(k)}^{\ (n-3)}\right) \quad (4.31)$$

At the sea-sand interface the matching conditions are defined as (Equation (4.32) is for the pressure match condition and Equation (4.33) is for the vertical velocity match condition);

$$\varphi_i^{(n+1)} - \psi_i^{(n+1)} = \underbrace{\varphi_i^{(n)} - \psi_i^{(n)} \left(\frac{\delta t}{24}\right)\left(55\psi_i^{(n)} - 59\psi_i^{(n-1)} + 37\psi_i^{(n-2)} - 9\psi_i^{(n-3)}\right)}_{R_4} \quad (4.32)$$

$$f_{ij}^{\ z} f_{jk}^{\ -1} \varphi_k^{\ n+1} - f_{ij}^{\ z} f_{jk}^{\ -1} \psi_k^{\ n+1} = 0 \quad (4.33)$$

On the left and right vertical faces of the sand domain, governing equation exists and it is formulated as;

$$\left(f_{ij}^{\ xx} + f_{ij}^{\ zz}\right) f_{jk}^{\ -1} \varphi_k^{\ n+1} = 0 \quad (4.34)$$

At the bottom of the sand domain, the no-vertical-flow condition is defined as;

$$f_{ij}^{\ z} f_{jk}^{\ -1} \varphi_k^{\ n+1} = 0 \quad (4.35)$$

Now the system of equations is set and the boundary value problem in matrix form becomes;

$$\begin{pmatrix} 1 & 0 & 0 & 0 & 0 & 0 & 0 & 0 \\ 0 & 1 & 0 & 0 & 0 & 0 & 0 & 0 \\ 0 & 0 & 1 & 0 & 0 & 0 & 0 & 0 \\ 0 & 0 & 0 & 1 & 0 & 0 & 0 & 0 \\ 0 & 0 & 0 & f^z f^{-1} & f^z f^{-1} & 0 & 0 & 0 \\ 0 & 0 & 0 & 0 & 0 & f_{xx} + f_{zz} & 0 & 0 \\ 0 & 0 & 0 & 0 & 0 & 0 & f_{xx} + f_{zz} & 0 \\ 0 & 0 & 0 & 0 & 0 & 0 & 0 & f^z \end{pmatrix} \begin{Bmatrix} \varphi_1^{\ k+1} \\ \varphi_2^{\ k+1} \\ \varphi_3^{\ k+1} \\ \varphi_4^{\ k+1} \\ \psi_5^{\ k+1} \\ \psi_6^{\ k+1} \\ \psi_7^{\ k+1} \\ \psi_8^{\ k+1} \end{Bmatrix} = \begin{Bmatrix} \varphi_1^{\ *k+1} \\ \varphi_2^{\ *k+1} \\ \varphi_3^{\ *k+1} \\ R_4 \\ 0 \\ 0 \\ 0 \\ 0 \end{Bmatrix} \quad (4.36)$$

4.6. Solutions of Wave Dispersion Relations for Impervious and Pervious Sea Beds

Wave dispersion relation can be regarded as the primary characteristic defining the behavior of a wave by relating angular frequency (ω) and wave number (k). The wave motion is specified by the four parameters H , T , h and L (wave height, wave period,

water depth and wavelength). However, these four parameters are dependent on each other and three parameters should be specified to uniquely specify a wave.

In Chapter 3, the dispersion relations for waves passing over horizontal and impervious sea bed and waves passing over pervious sea bed are determined. The solution of the first one is relatively easier than the second one because in the first one, the wave number is a real number and easy to determine with the existing formulas. The dispersion equation for waves passing over impervious sea bed was determined from the linear wave theory;

$$\omega^2 = g\,k\,\tanh(kh) \tag{4.37}$$

Hunt (1979) obtained an approximation for wave dispersion relation in the following form;

$$(kh)^2 = (\omega^2 h/g)^2 + \frac{\omega^2 h/g}{1+\sum_{n=1}^{\infty} h_n (\omega^2 h/g)^n} \tag{4.38}$$

This expression is a remarkably accurate approximation to Equation (4.37) over all wave lengths. Indeed, it was derived so as to be exact in both long and short wave limits. Venezian (1979) discusses to Hunt (1979) "The resulting expression with six constants gives answers with a maximum error of 0.008%" over an entire range of k .

where h_n are given by;

$$\begin{aligned} h_1 &= 0.6666666667 \\ h_2 &= 0.3555555556 \\ h_3 &= 0.1608465608 \\ h_4 &= 0.0632098765 \\ h_5 &= 0.0217540484 \\ h_6 &= 0.0065407983 \end{aligned} \tag{4.39}$$

This expression is an accurate approximation for wave dispersion relation for all wavelengths. The equation and the coefficients above are implemented in the code without difficulty.

For waves passing over pervious sea beds, the wave dispersion relation was determined as;

$$\frac{\omega^2}{gk\tanh kh} = 1 + i\frac{\omega K}{g}\tanh kh_d\left(\coth kh - \frac{\omega^2}{gk}\right) \tag{4.40}$$

K is the permeability of the sand layer and h_d is the thickness of the sand layer. It should be noted that the dispersion relation above modifies to the dispersion relation over impervious sea bed when $K = 0$. Here, the wave number is complex;

$$k = k_r + ik_i \tag{4.41}$$

Multiplying (4.40) by $k\tanh kh$;

$$\underset{\alpha}{\frac{\omega^2}{g}} = k\tanh kh + i\underbrace{\left(\frac{\omega K}{g}\right)}_{\beta}k\tanh kh_d\left[1 - \underset{\alpha}{\left(\frac{\omega^2}{g}\right)}\frac{\tanh kh}{k}\right]$$

$$\begin{aligned}\alpha &= k\tanh kh + i\beta k\tanh kh_d\left[1 - \alpha\frac{\tanh kh}{k}\right] \\ &= k\tanh kh + i\beta\tanh kh_d\left[k - \alpha\tanh kh\right]\end{aligned} \tag{4.42}$$

Let,

$$T_r + iT_i = \tanh(k_r + ik_i) \tag{4.43}$$

and

$$\tau_r + i\tau_i = \tanh(k_r + ik_i)h_d \tag{4.44}$$

Rewriting Equation (4.42) in view of Equations (4.41), (4.43) and (4.44), we have,

$$\begin{aligned}\alpha &= (k_r + ik_i)(T_r + iT_i) + i\beta(\tau_r + i\tau_i)\left[(k_r + ik_i) - \alpha(T_r + iT_i)\right] \\ &= (k_r + ik_i)(T_r + iT_i) + \ i\beta\tau_r - \beta\tau_i\ \left[(k_r + ik_i) - \alpha(T_r + iT_i)\right] \\ &= (k_r + ik_i)(T_r + iT_i) + \ i\beta\tau_r - \beta\tau_i\ \left[(k_r - \alpha T_r) + i(k_i - \alpha T_i)\right] \\ &= k_rT_r - k_iT_i + ik_iT_r + ik_rT_i + i\beta\tau_r(k_r - \alpha T_r) + i\beta\tau_r i(k_i - \alpha T_i) \\ &\quad -\beta\tau_i(k_r - \alpha T_r) - \beta\tau_i i(k_i - \alpha T_i) \\ &= k_rT_r - k_iT_i - \beta\tau_r(k_i - \alpha T_i) - \beta\tau_i(k_r - \alpha T_r) + i[k_iT_r + k_rT_i \\ &\quad +\beta\tau_r(k_r - \alpha T_r) - \beta\tau_i(k_i - \alpha T_i)]\end{aligned} \tag{4.45}$$

Collecting real and imaginary parts of Equation (4.45) yields two transcendental equations in the unknowns k_r and k_i,

$$\begin{aligned} k_r T_r - k_i T_i - \beta k_r \tau_i - \beta k_i \tau_r + \alpha\beta T_r \tau_i + \alpha\beta T_i \tau_r - \alpha = 0 \\ k_r T_i + k_i T_r - \beta k_i \tau_i + \beta k_r \tau_r + \alpha\beta T_i \tau_i - \alpha\beta T_r \tau_r = 0 \end{aligned} \tag{4.46}$$

Noting that,

$$\tanh ik_i h = i \tan k_i h \tag{4.47}$$

It is obtained that,

$$\begin{aligned} \tanh kh &= \tanh(k_r + ik_i)h \\ &= \frac{\tanh k_r h + \tanh ik_i h}{1 + \tanh k_r h \tanh ik_i h} \end{aligned} \tag{4.48}$$

(4.47) can be written as,

$$\begin{aligned} \tanh kh &= \frac{(1 - i\tanh k_r h \tan k_i h)}{(1 - i\tanh k_r h \tan k_i h)} \left(\frac{\tanh k_r h + i \tan k_i h}{1 + i\tanh k_r h \tan k_i h} \right) \\ &= \frac{(\tanh k_r h + k_i \tan^2 k_i h \tanh k_r h) + i(\tan k_i h - \tanh^2 k_r h \tan k_i h)}{1 + \tanh^2 k_r h \tan^2 k_i h} \end{aligned} \tag{4.49}$$

In view of Equations (4.43) and (4.44),

$$\begin{aligned} T_r &= \frac{\tanh k_r h + k_i \tan^2 k_i h \tanh k_r h}{1 + \tanh^2 k_r h \tan^2 k_i h} \\ T_i &= \frac{\tan k_i h - \tanh^2 k_r h \tan k_i h}{1 + \tanh^2 k_r h \tan^2 k_i h} \end{aligned} \tag{4.50}$$

and,

$$\begin{aligned} \tau_r &= \frac{\tanh k_r h_d + k_i \tan^2 k_i h_d \tanh k_r h_d}{1 + \tanh^2 k_r h_d \tan^2 k_i h_d} \\ \tau_i &= \frac{\tan k_i h_d - \tanh^2 k_r h_d \tan k_i h_d}{1 + \tanh^2 k_r h_d \tan^2 k_i h_d} \end{aligned} \tag{4.51}$$

The analytical solution gave us that,

$$\eta = ae^{k_i x} e^{-i(k_r x - \omega t)} \tag{4.52}$$

Since the wave frequency ω is real, the real part of the wave number, k_r, should satisfy the wave dispersion equation

$$\omega^2 = gk_r \tanh k_r h \tag{4.53}$$

Knowing k_r, we then need only to find k_i. However, in order to verify the derivation of the Equation (4.46), we will find both k_r and k_i iteratively and then compare the k_r value with the root of Equation (4.52).

Among the methods for determining the roots of transcendental equations, the fixed point iteration method is the easiest one to implement. However, the form of the equations to be iterated must be chosen so that the iterations are convergent and the initial estimates of the roots must be close to the actual roots.

For a reasonable approximation, k_r is taken from the solution of the dispersion equation for waves over impervious sea bed. To determine a reasonable approximation for k_i, the sand layer can be assumed to have a very large thickness so that $\tanh kd \to 1$ and the wave is assumed to be in shallow water. With these assumptions, the wave dispersion relationship becomes,

$$\begin{aligned} \frac{\omega^2}{gk(kh)} &= 1 + i\frac{\omega K}{g}\left(\frac{1}{kh} - \frac{\omega^2}{gk}\right) \\ &= 1 + i\frac{\omega K}{g}\left(\frac{1}{kh}\right)\left(1 - \frac{\omega^2 h}{g}\right) \end{aligned} \tag{4.54}$$

Let $\mu = kh$ and $\Omega = \omega^2 h / g$ in Equation (4.54),

$$\begin{aligned} \frac{\omega^2}{gk\mu}\left(\frac{h}{h}\right) &= 1 + i\beta\left(\frac{1}{\mu}\right)\ 1 - \Omega \\ \frac{\omega^2 h}{g}\frac{1}{\mu(kh)} &= 1 + i\beta\left(\frac{1}{\mu}\right)\ 1 - \Omega \\ \frac{\Omega}{\mu^2} &= 1 + i\beta\left(\frac{1}{\mu}\right)\ 1 - \Omega \end{aligned} \tag{4.55}$$

The last equation is a quadratic equation in $\mu = kh$,

$$\mu^2 + i\beta(1-\Omega)\mu - \Omega = 0 \tag{4.56}$$

Solving for μ,

$$\mu = -i\frac{\beta}{2}(1-\Omega) \pm \frac{1}{2}\sqrt{\left[i\beta(1-\Omega)\right]^2 + 4\Omega} \tag{4.57}$$

To simplify (4.57), it is assumed that the waves under consideration have periods of $O(10^0) - O(10^1)$ seconds and that the water depths are in the range of $O(10^0) - O(10^{-1})$ meters. The permeability of sand is of $O(10^{-6})$ m/s. Noting that g is $O(10^1)$ m^2/s, it is obtained that,

$$\begin{aligned}
\omega &= \frac{2\pi}{T} = \frac{\mathrm{O}(10^0)}{\mathrm{O}(10^1), \mathrm{O}(10^0)} = \mathrm{O}(10^0) - \mathrm{O}(10^{-1}) \\
\beta &= \frac{\omega K}{g} = \frac{\left[\mathrm{O}(10^0), \mathrm{O}(10^{-1})\right]\mathrm{O}(10^{-6})}{\mathrm{O}(10^1)} \\
&= \mathrm{O}(10^{-7}) - \mathrm{O}(10^{-8}) \\
\Omega &= \frac{\omega^2 h}{g} = \frac{\left[\mathrm{O}(10^0), \mathrm{O}(10^{-2})\right]\left[\mathrm{O}(10^0), \mathrm{O}(10^{-1})\right]}{\mathrm{O}(10^1)} \\
&= \mathrm{O}(10^{-1}) - \mathrm{O}(10^{-4}) \\
\beta^2(1-\Omega)^2 &= \mathrm{O}\left(\left[10^{-14}, 10^{-16}\right]\left[10^0, 10^{-1}, 10^{-4}, 10^{-2}, 10^{-8}\right]\right) \\
&= \mathrm{O}(10^{-14}) - \mathrm{O}(10^{-24})
\end{aligned} \tag{4.58}$$

From the order of magnitudes analysis, it can be determined that,

$$\mathrm{O}\left[\beta^2(1-\Omega)^2\right] = \mathrm{O}[\Omega] \tag{4.59}$$

Then Equation (4.57) can be simplified to,

$$\mu = (k_r + ik_i)h = -i\frac{\beta}{2}(1-\Omega) \pm \sqrt{\Omega} \tag{4.60}$$

For $k_r > 0$, the real part of the equation above should be positive. Therefore, the plus sign is chosen, that is

$$\mu = (k_r + ik_i)h = -i\frac{\beta}{2}(1-\Omega) + \sqrt{\Omega} \tag{4.61}$$

Equating real and imaginary parts,

$$k_r h = \sqrt{\Omega} = \sqrt{\frac{\omega^2 h}{g}} \tag{4.62}$$

and,

$$\begin{aligned} k_i h &= -\frac{\beta}{2}(1-\Omega) \\ &= \frac{1}{2}\frac{\omega K}{g}\left(\frac{\omega^2 h}{g} - 1\right) \\ &= \frac{1}{2}\frac{\omega K}{g}\left[\ k_r h\ ^2 - 1\right] \end{aligned} \tag{4.63}$$

If the sand layer is impervious and the waves are in the shallow water, the dispersion relation in shallow water can be written as,

$$\frac{w^2 h}{g} = \kappa h \tanh \kappa h \xrightarrow{\kappa h \to 0} \frac{w^2 h}{g} = (\kappa h)^2 \tag{4.64}$$

In the equation above, $\kappa = k_r$ and comparing Equations (4.62) and (4.64) yields,

$$k_r = \kappa \tag{4.65}$$

Equation (4.65) suggests that the wave length is not affected by the porous bottom in shallow water. A reasonable first iterant for the set of equations given in Equation (4.46) can therefore be obtained by first determining $k_r h$ from the dispersion relationship for waves propagating over an impermeable sea bed and then using this value in Equation (4.63) to obtain $k_i h$.

4.7. Implementation of the Fixed Point Iteration Scheme

For the fixed point iteration of Equation (4.46), one way to write the equations is,

$$\begin{aligned} k_r(T_r - \beta\tau_i) &= k_i T_i + \alpha + \beta k_i \tau_r - \alpha\beta(\tau_r T_i + \tau_i T_r) \\ k_i(T_r - \beta\tau_i) &= -k_r T_i - \beta\tau_r k_r + \alpha\beta(\tau_r T_r - \tau_i T_i) \end{aligned} \tag{4.66}$$

or,

$$k_r = \frac{k_i T_i + \alpha + \beta k_i \tau_r - \alpha\beta(\tau_r T_i + \tau_i T_r)}{T_r - \beta\tau_i}$$
$$k_i = \frac{-k_r T_i - \beta\tau_r k_r + \alpha\beta(\tau_r T_r - \tau_i T_i)}{T_r - \beta\tau_i} \tag{4.67}$$

This choice was tried and it was found that while the iterations for k_r converged, those for k_i oscillated about $k_i = 0$ without convergence. As a second choice, the first equation of (4.67) was retained while the second equation was modified. The new set of equations is,

$$k_r = \frac{k_i T_i + \alpha + \beta k_i \tau_r - \alpha\beta(\tau_r T_i + \tau_i T_r)}{T_r - \beta\tau_i} \tag{4.68}$$

$$k_i = -\frac{(k_r T_i - \beta k_i \tau_i + \beta k_r \tau_r + \alpha\beta T_i \tau_i - \alpha\beta T_r \tau_r)}{T_r} \tag{4.69}$$

This set proved to be convergent for both the unknowns. The algorithm used for the solution is as follows:

(i) Use Hunt's (1979) approximation to determine the initial iterant $k_r^{(old)}$.

(ii) Use $k_r^{(old)}$ in (4.63) to determine the initial iterant $k_i^{(old)}$.

(iii) Use $k_r^{(old)}$ and $k_i^{(old)}$ in (4.68) and (4.69) to determine $k_r^{(new)}$ and $k_i^{(new)}$.

(iv) If $\left|k_r^{(new)} - k_r^{(old)}\right| \le \varepsilon$ and $\left|k_i^{(new)} - k_i^{(old)}\right| \le \varepsilon$, convergence is achieved.

(v) If the conditions above are not satisfied, then let $k_r^{(old)} \leftarrow k_r^{(new)}$, $k_i^{(old)} \leftarrow k_i^{(new)}$ and go to the third step for the next iteration.

The following figure shows the convergence of the imaginary part of the wave number for the wave parameters presented in the table below.

In order to verify the claims made here, a numerical example is given with the following data: $T = 4.5$s, $h = 2$m, $l = 4$m, $d = h + l = 6$m and $K = 10^{-6}$ m/s. The initial iterants found are,

$$k_r = 0.3376882 \qquad k_i = -0.1935222 \times 10^{-7}$$

Convergence for both unknowns was achieved in 46 iterations using $\varepsilon = 1 \times 10^{-12}$. The final values of the unknowns are;

$$k_r = 0.3376879 \qquad k_i = -0.2946055 \times 10^{-7}$$

The progress of the iterations is shown in the figure (4.5).

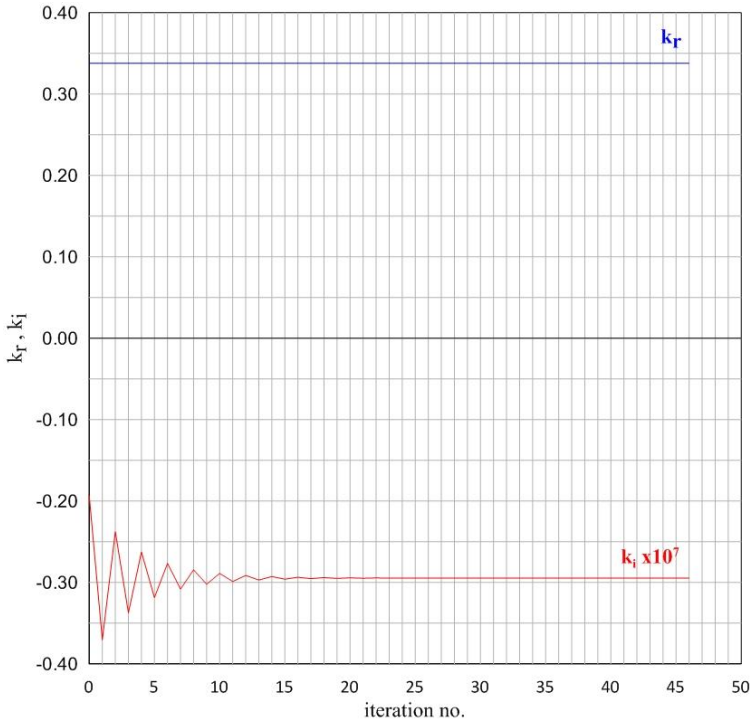

Figure 4.5. Convergence of real and imaginary parts of the wave number.

4.8. Rippled Sea Beds

As mentioned in the introduction, there are four stages of the study at hand which are wave propagation over impermeable and horizontal sea bed, wave propagation over impermeable and rippled sea bed, wave propagation over permeable and horizontal sea bed and wave propagation over permeable and rippled sea bed.

For the rippled sea bed geometry, the following criteria which Nielsen (1979), according to field experiments, stated is used;

$$H_r / L_r = 0.2 \tag{4.70}$$

The following figure is taken from Nielsen (1979), showing the experimental results;

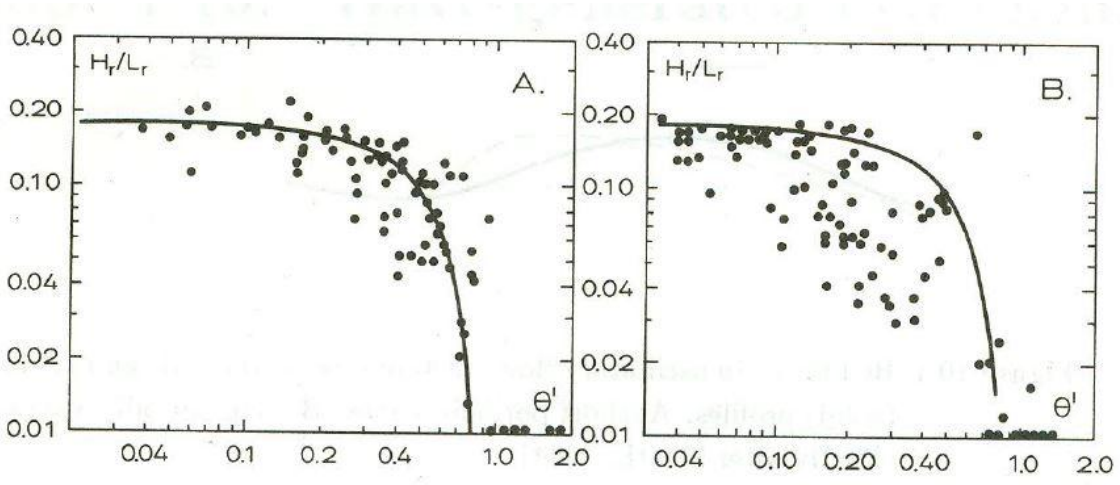

Figure 4.6. Experimental results for ripple steepness (Nielsen 1979).

Equation (4.70) gives the upper bound of the ratio of the height of the sea bed ripples and the length of the sea bed ripples regarding the stability of the models created. The ripples are included to the present model geometry as a sinusoidal wave. The following figure shows the rippled sea bed used in this study for a ripple height of 0.04 meters and a ripple length of 0.2 meters;

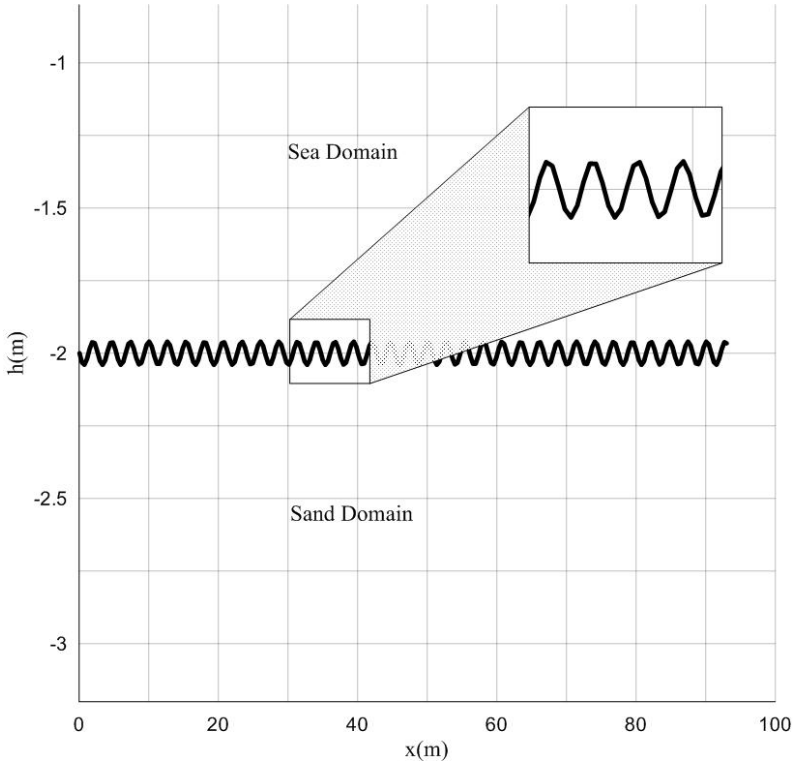

Figure 4.7. Rippled sea bed in the models.

5. NUMERICAL TESTS AND RESULTS

5.1. Overview

In this chapter, numerical tests and the corresponding results are presented. As mentioned in earlier chapters, the four stages of this study are wave propagation over impermeable and horizontal sea bed, wave propagation over impermeable and rippled sea bed, wave propagation over permeable and horizontal sea bed and wave propagation over permeable and rippled sea bed. Numerical tests and results are presented following this order and for each case; some important physical parameters and model parameters are tabulated before presenting results.

In Sections 5.2 and 5.3, free surface displacements, velocity potentials at the free surface and at the sea bed, dynamic pressures at the sea bed are presented. Presented results are compared with the analytical results.

In Sections 5.4 and 5.5, wave propagation over permeable and horizontal/rippled sea bed, free surface displacements, velocity potentials in sea and sand zones, dynamic pressures at the sea bed are presented. Contour plots and velocity vectors are also presented in these sections for constructing the basis for a future advection-diffusion model inside a sandy sea bed.

It should be noted that results for latter two cases are plotted starting at half a wavelength inside the right and left boundaries since the left and right hand side boundary conditions for the sand are not clearly defined in the literature or in related academic studies. As stated in the formulation section, the continuity equation is defined on the left and right hand side boundaries of the sand domain. However; the results for wave propagations over pervious sea bed are somewhat deformed by defining the continuity equation on the left and right boundaries of the sand zone. Therefore; it is preferred to present these results starting at half a wavelength from left and right boundaries of the sand zone.

5.2. Wave Propagation over Impervious and Horizontal Sea Bed

Table 5.1. Physical Parameters

Wave Period (T)	4.5 s.
Wave Height (H)	1.1 m
Relative Depth (h/L)	0.113
Wave Number (k)	0.34
Wave Steepness (H/L)	0.062
Wave Celerity (c)	3.9 m/s

Table 5.2. Model Parameters

Total number of nodes on the boundaries	258
Number of Waves inside solution domain	2
Run time	5T

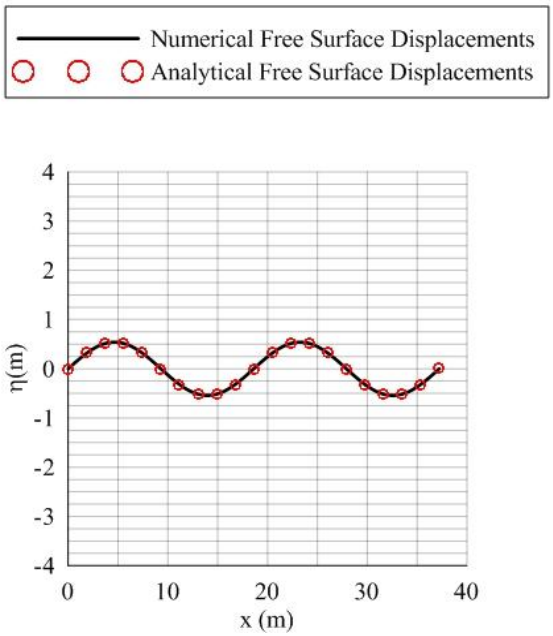

Figure 5.2. Free surface displacements.

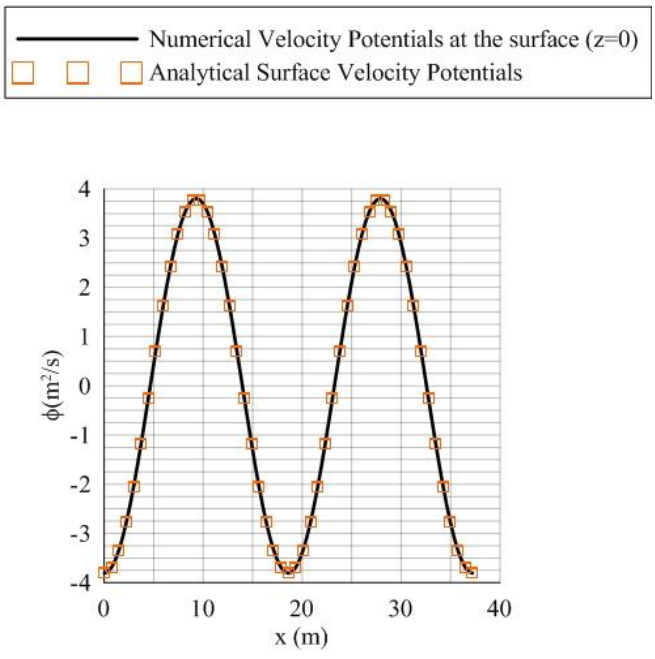

Figure 5.1. Velocity potentials (z=0).

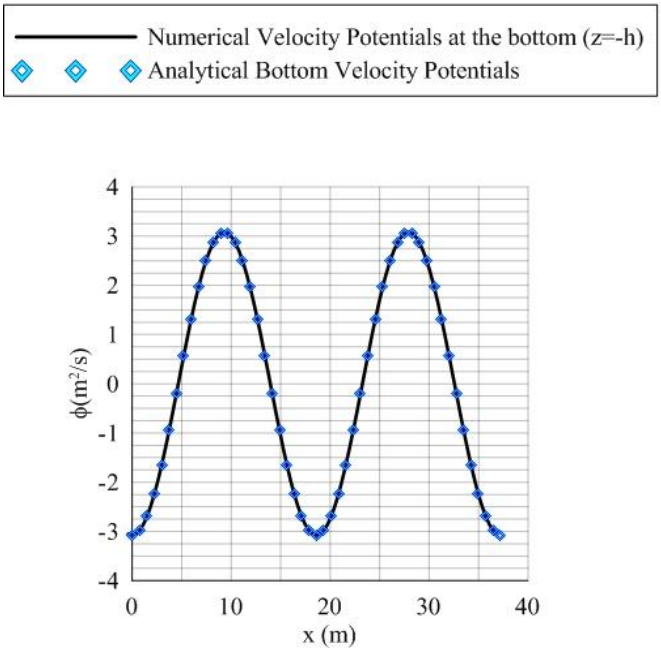

Figure 5.4. Velocity potentials (z=-h).

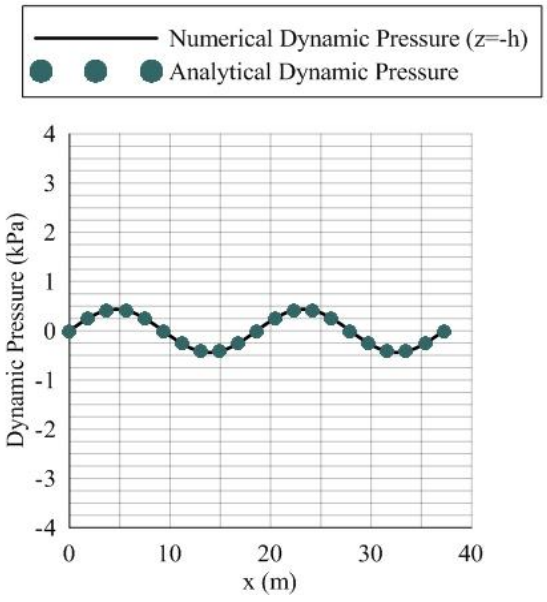

Figure 5.3. Dynamic pressures (z=-h).

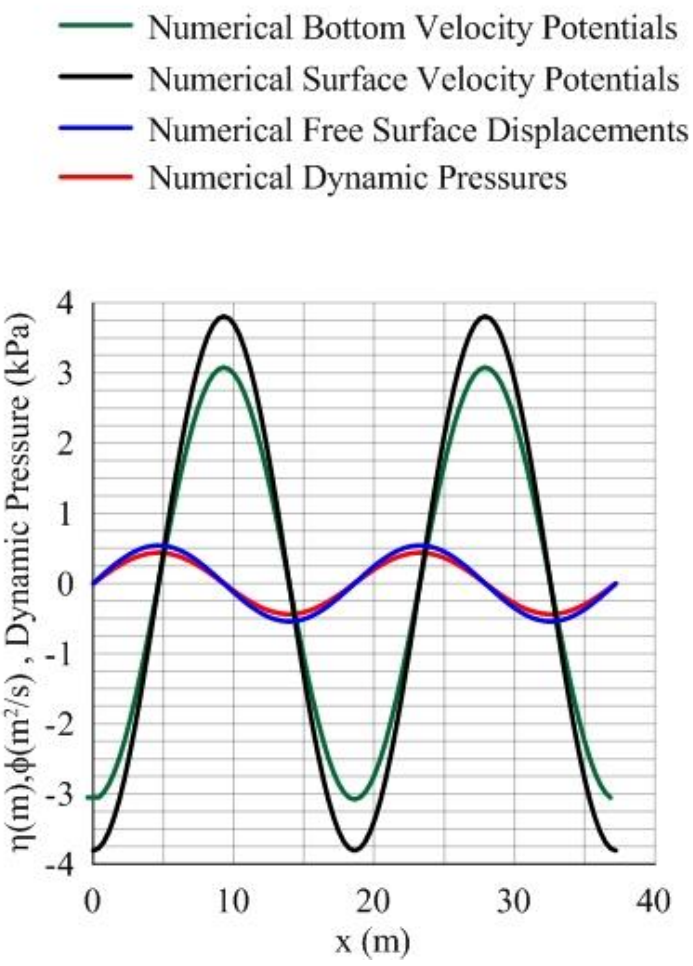

Figure 5.5. Numerical results for horizontal and impervious sea bed.

5.3. Wave Propagation over Impervious and Rippled Sea Bed

Table 5.3. Physical Parameters

Wave Period (T)	4.5 s.
Wave Height (H)	1.1 m
Relative Depth (h/L)	0.113
Wave Number (k)	0.34
Wave Steepness (H/L)	0.062
Wave Celerity (c)	3.92 m/s
Ripple Height (H_r)	0.04 m
Ripple Length (L_r)	0.2 m

Table 5.4. Model Parameters

Total number of nodes on the boundaries	258
Number of Waves inside solution domain	2
Run time	5*T*

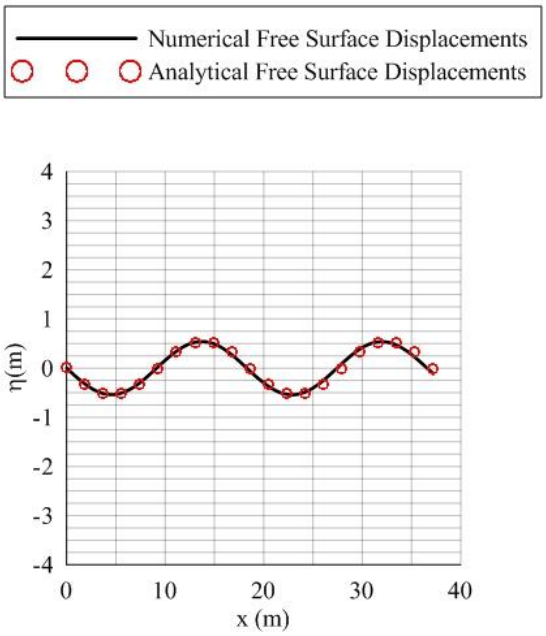

Figure 5.6. Free surface displacements.

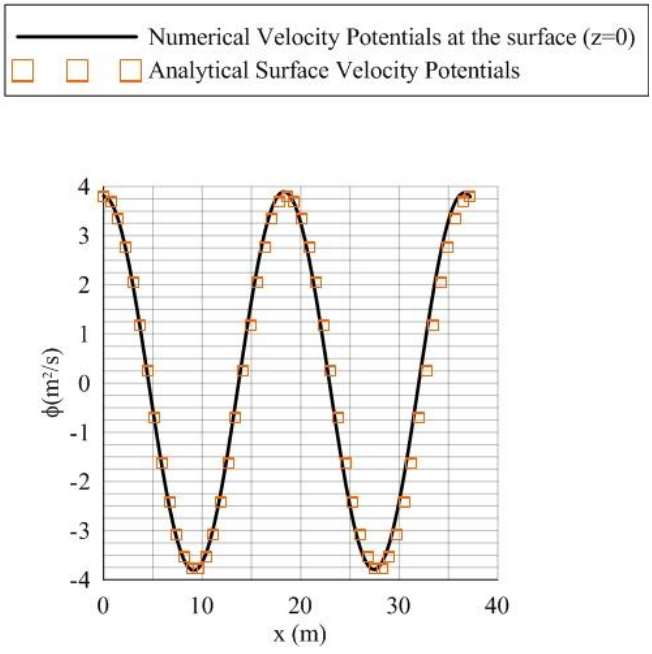

Figure 5.7. Velocity potentials (z=0).

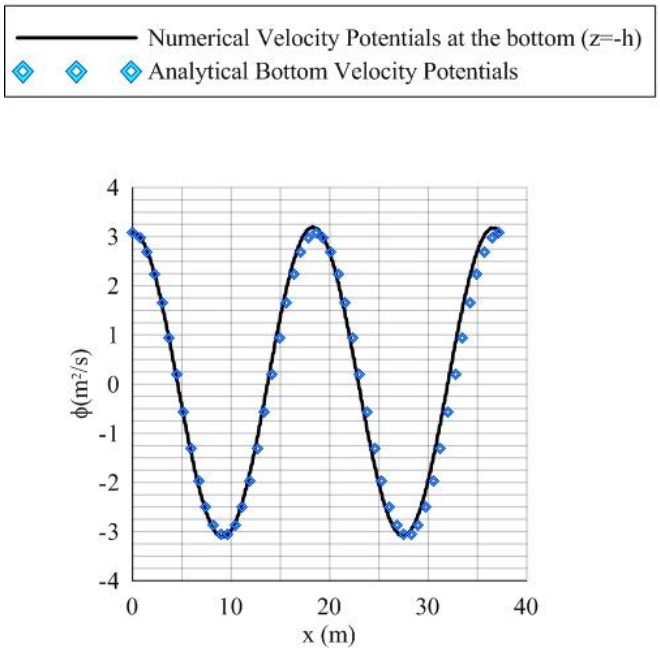

Figure 5.9. Velocity potentials (z=-h).

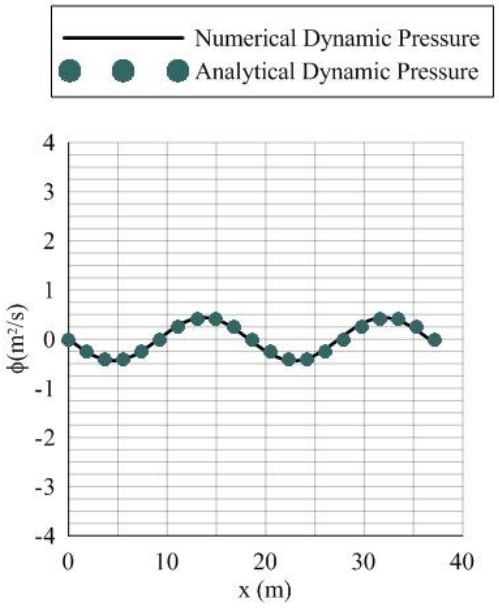

Figure 5.8. Dynamic pressure (z=-h).

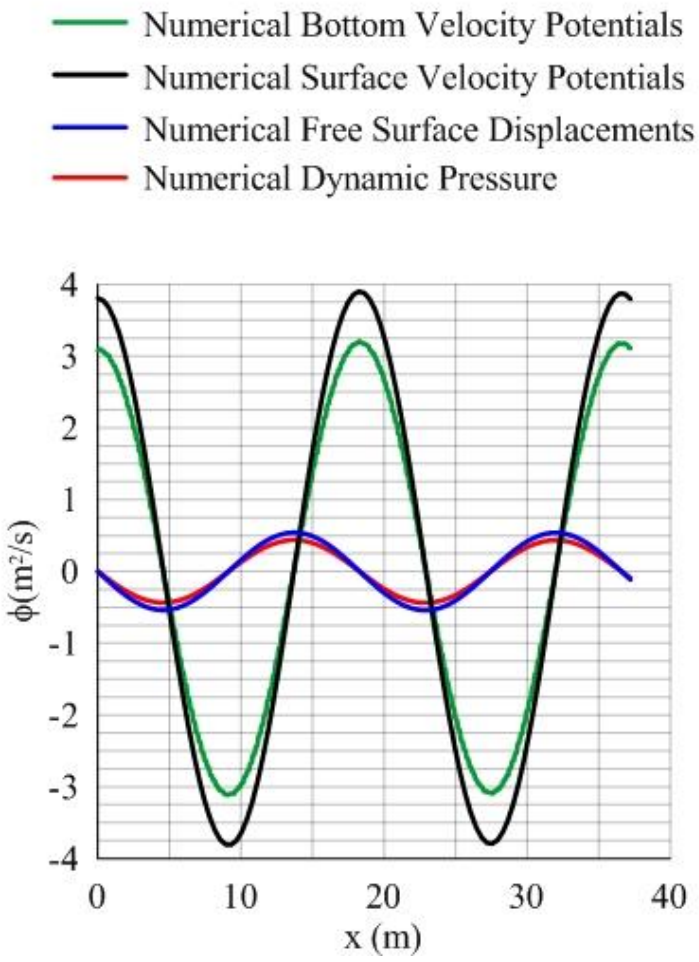

Figure 5.10. Numerical results for rippled and impervious sea bed.

5.4. Wave Propagation over Horizontal and Pervious Sea Bed

Table 5.5. Physical Parameters

Wave Period (T)	4.5 s.
Wave Height (H)	0.96 m
Relative Depth (h/L)	0.107
Wave Number $(k_r + k_i)$	$0.34 - 0.3*10^{-7}$i
Wave Steepness (H/L)	0.062
Wave Celerity (c)	3.92 m/s
Sand Zone Depth (d)	2 m
Permeability Coefficient (K)	10^{-6} m/s

Table 5.6. Model Parameters

Total number of nodes on the boundaries	516
Number of Waves inside solution domain	2
Run time	5T

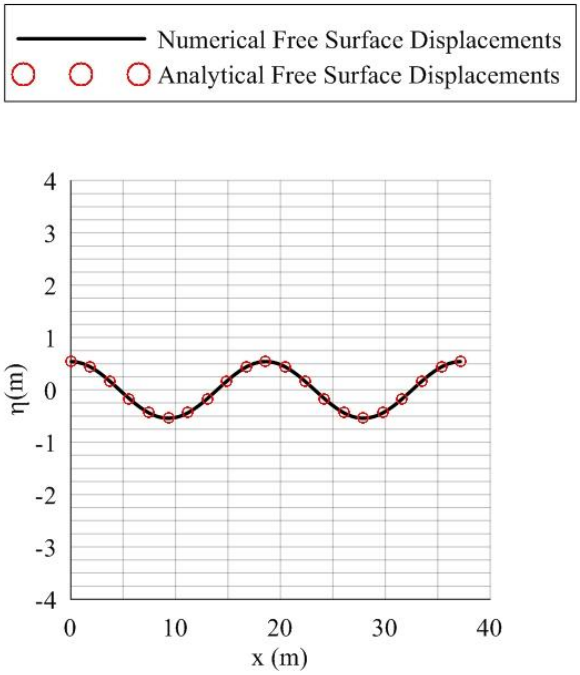

Figure 5.12. Free surface displacements.

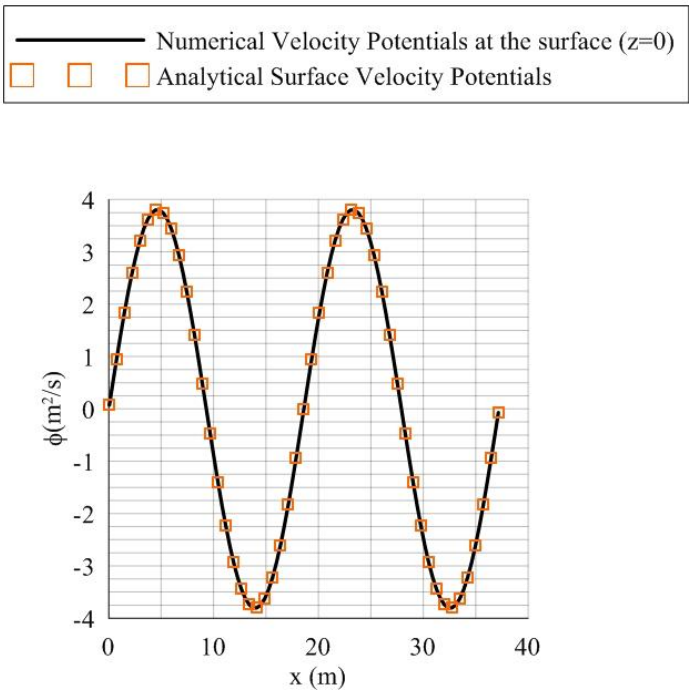

Figure 5.11. Velocity potentials (z=0).

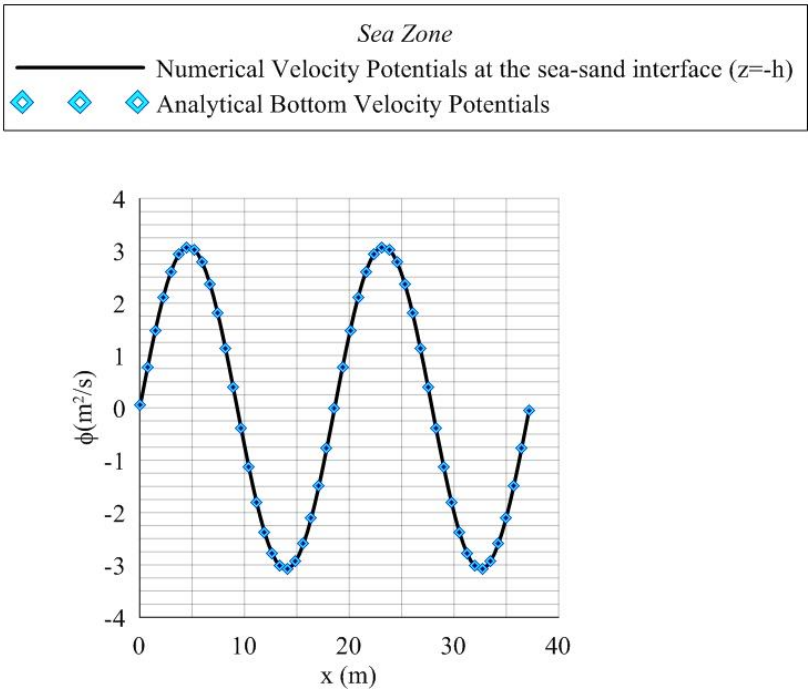

Figure 5.14. Velocity potentials in sea zone (z=-h).

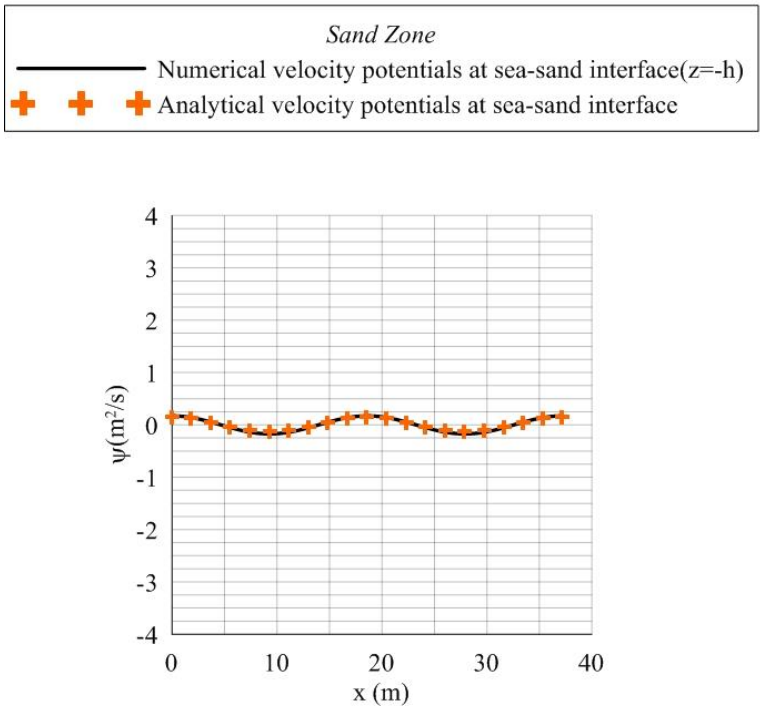

Figure 5.13. Velocity potentials in sand zone (z=-h).

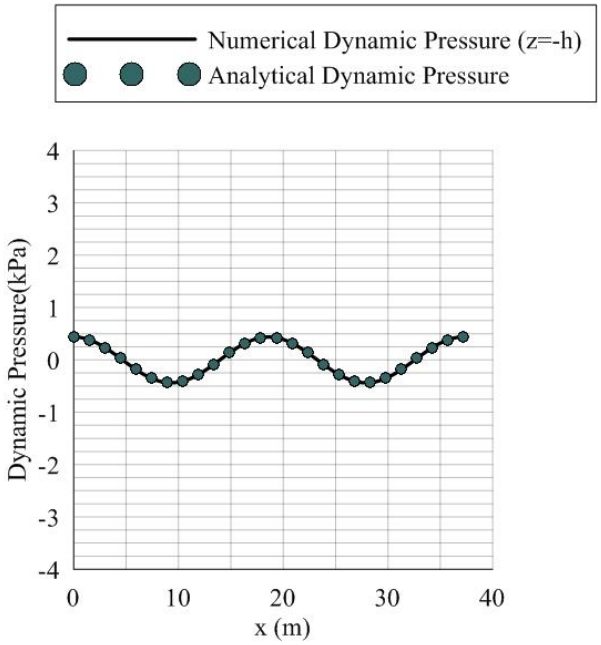

Figure 5.16. Dynamic pressures (z=-h).

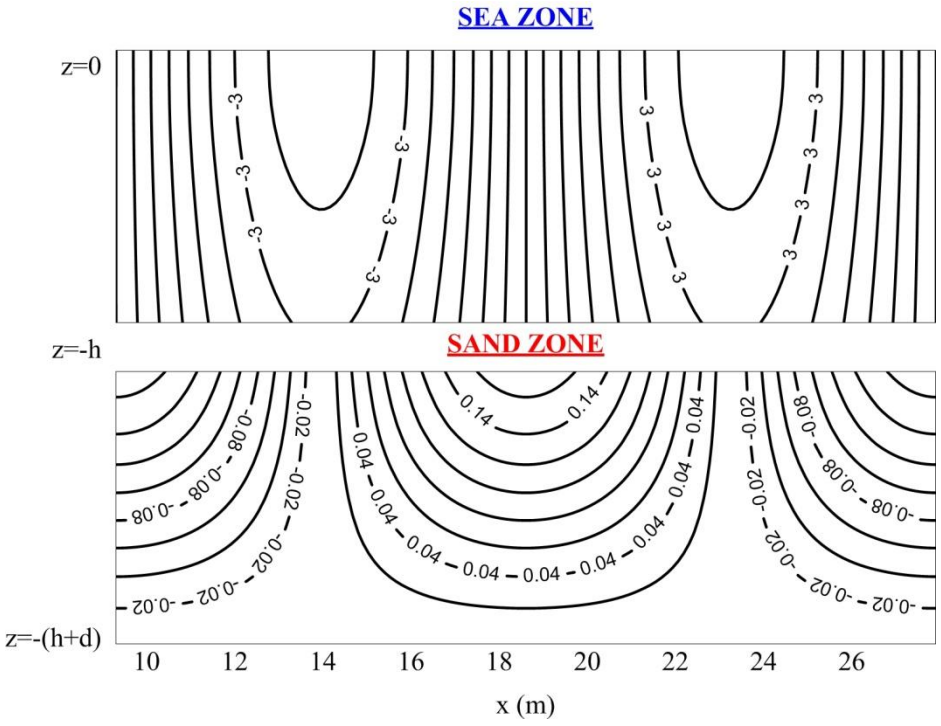

Figure 5.15. Contours of RBFCM interpolated velocity potentials.

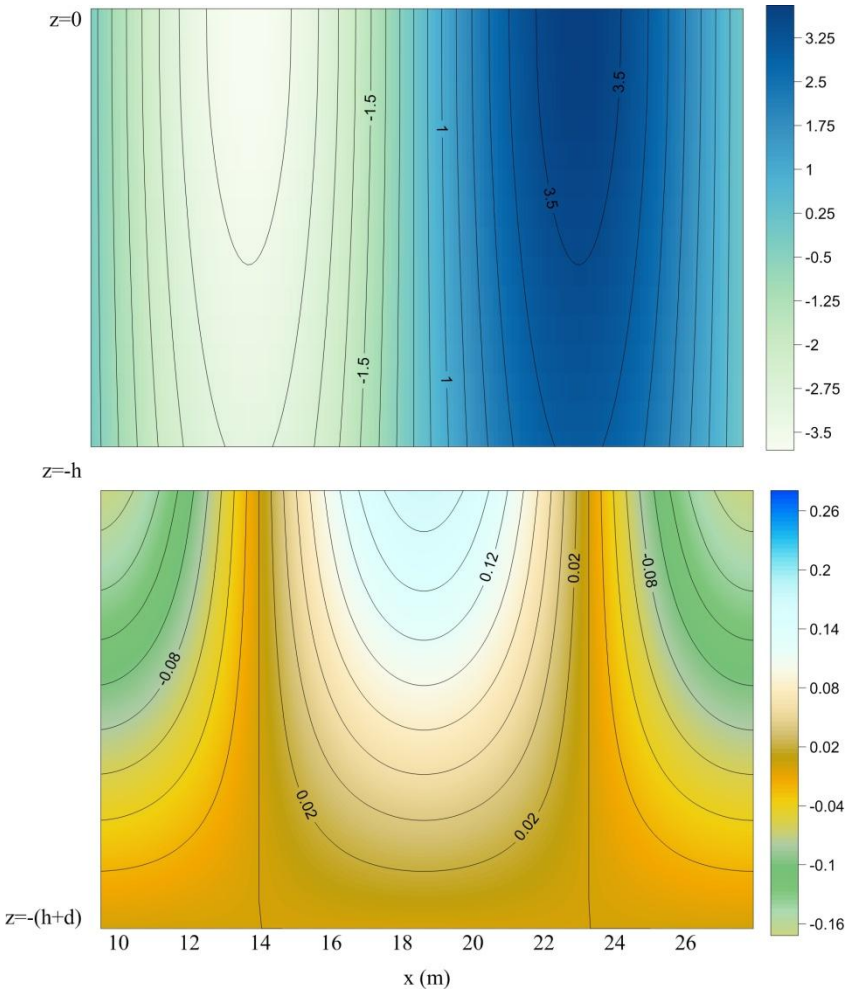

Figure 5.17. Image plot of velocity vectors in sea and sand zones.

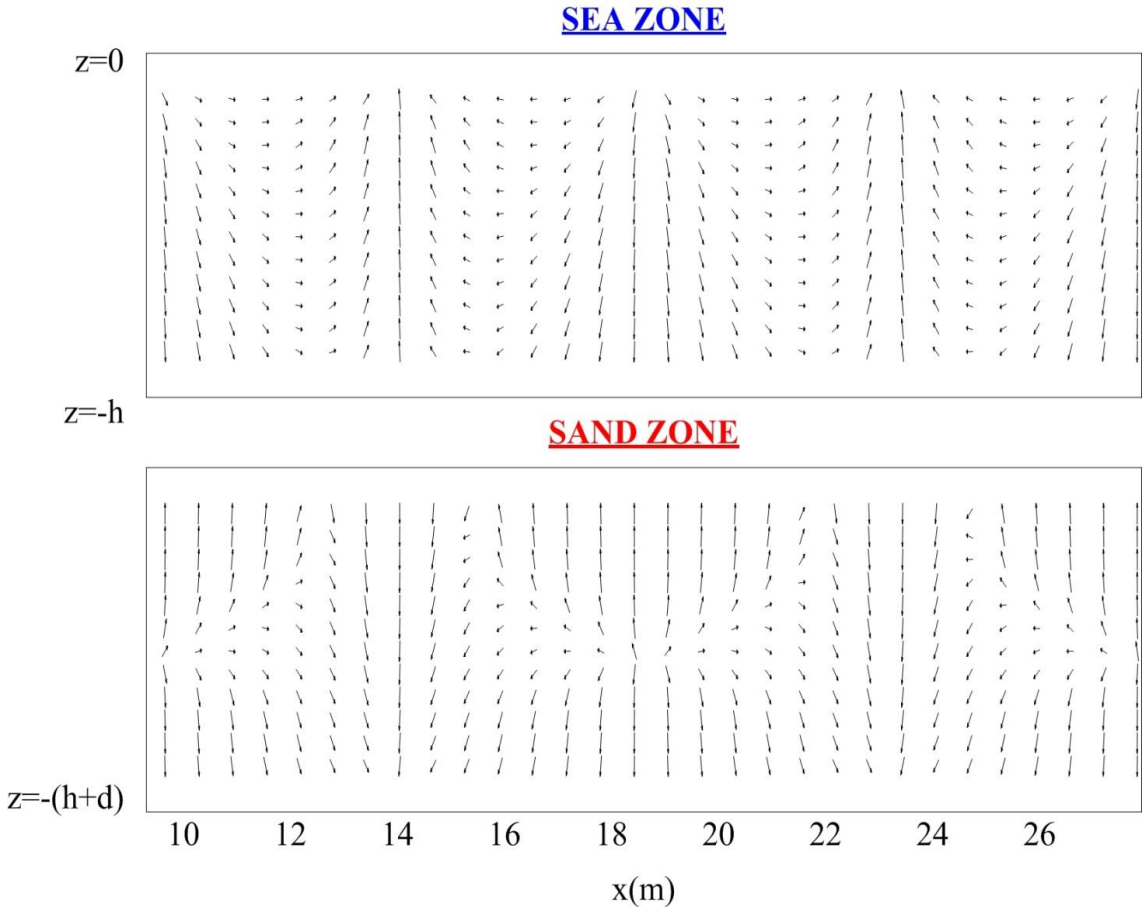

Figure 5.18. Velocity vectors.

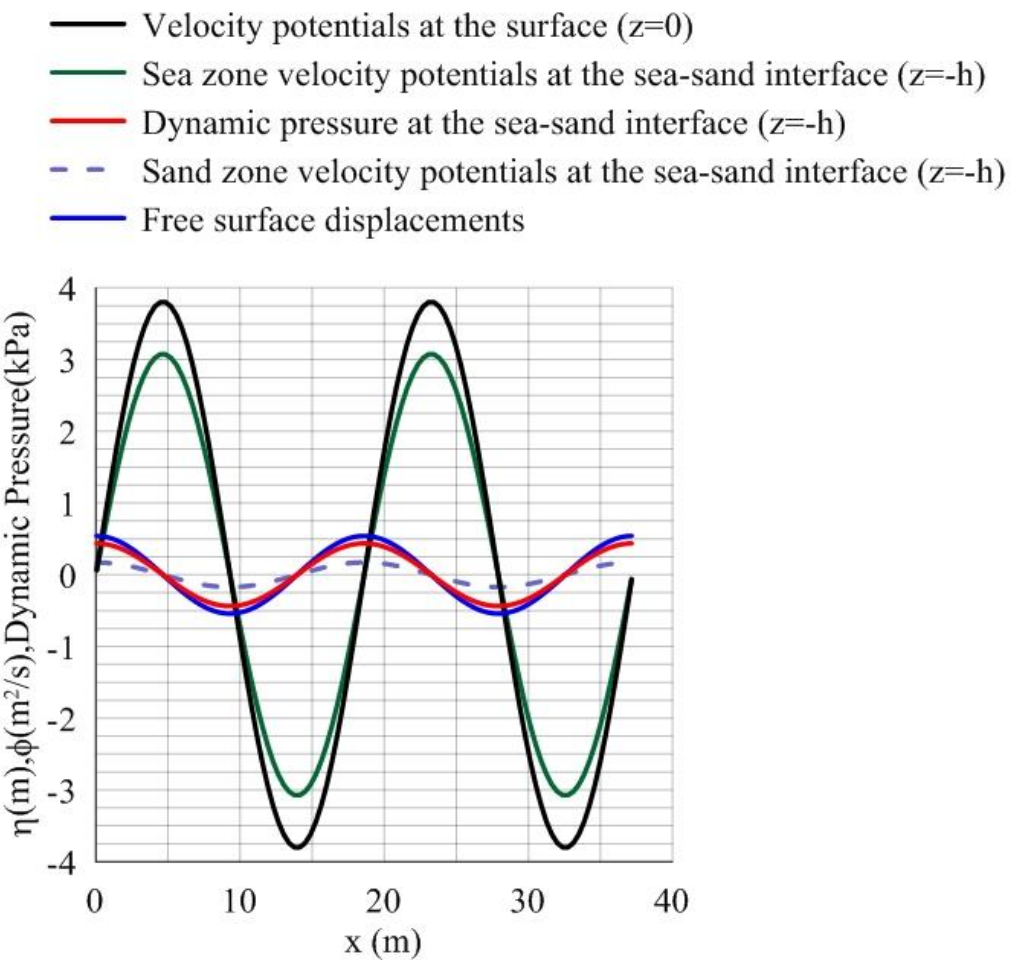

Figure 5.19. Numerical results for horizontal and pervious sea bed.

5.5. Wave Propagation over Rippled and Pervious Sea Bed

Table 5.7. Physical Parameters

Wave Period (T)	4.5 sec
Wave Height (H)	0.96 m
Relative Depth (h/L)	0.107
Wave Number $(k_r + k_i)$	$0.34 - 0.3*10^{-7}$i
Wave Steepness (H/L)	0.062
Wave Celerity (c)	3.92 m/s
Sand Zone Depth (d)	2 m
Permeability Coefficient (K)	10^{-6} m/s
Ripple Height (H_r)	0.04 m
Ripple Length (L_r)	0.2 m

Table 5.8. Model Parameters

Total number of nodes on the boundaries	516
Number of Waves inside solution domain	2
Run time	5T

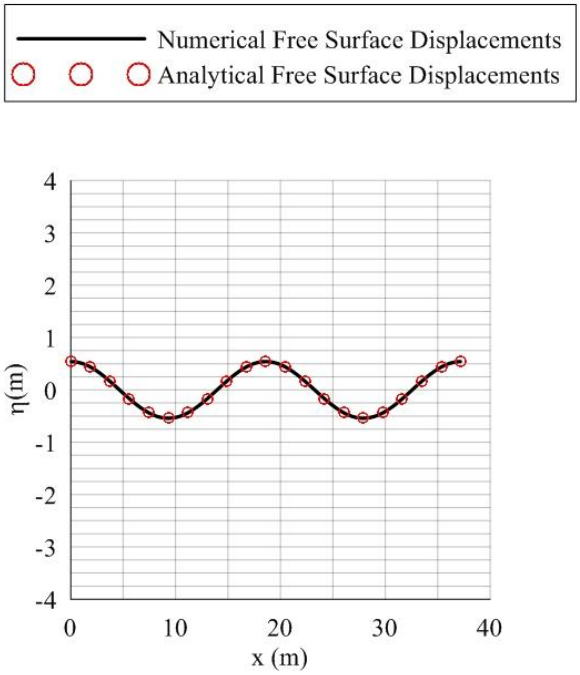

Figure 5.21. Free surface displacements.

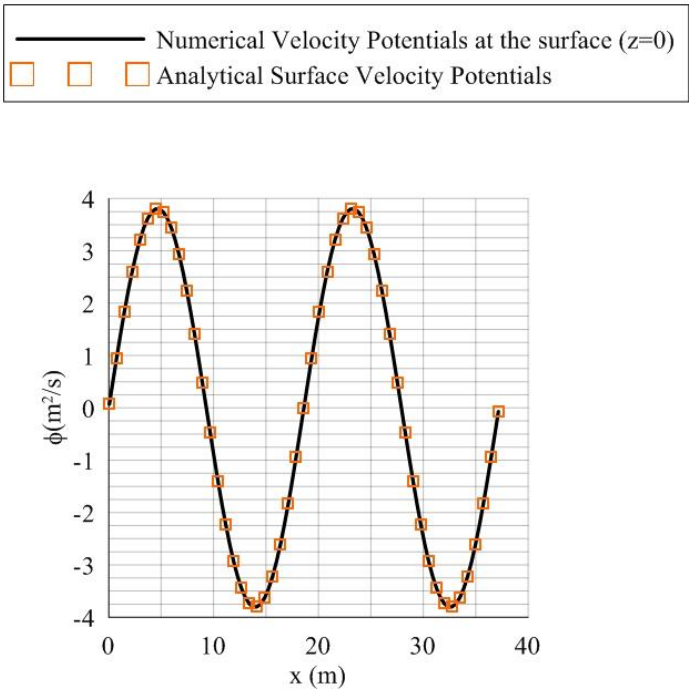

Figure 5.20. Velocity potentials (z=0).

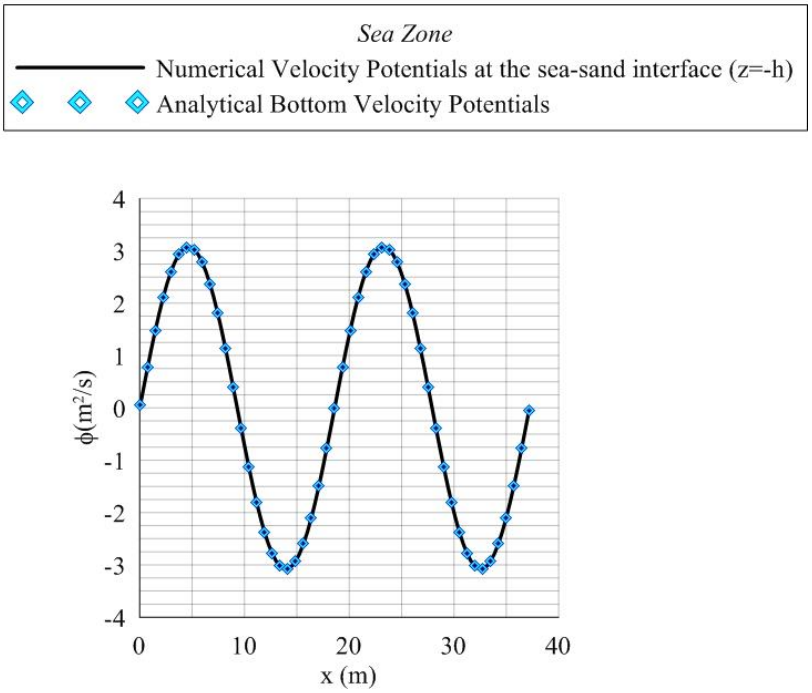

Figure 5.23. Velocity potenitals in sea zone (z=-h).

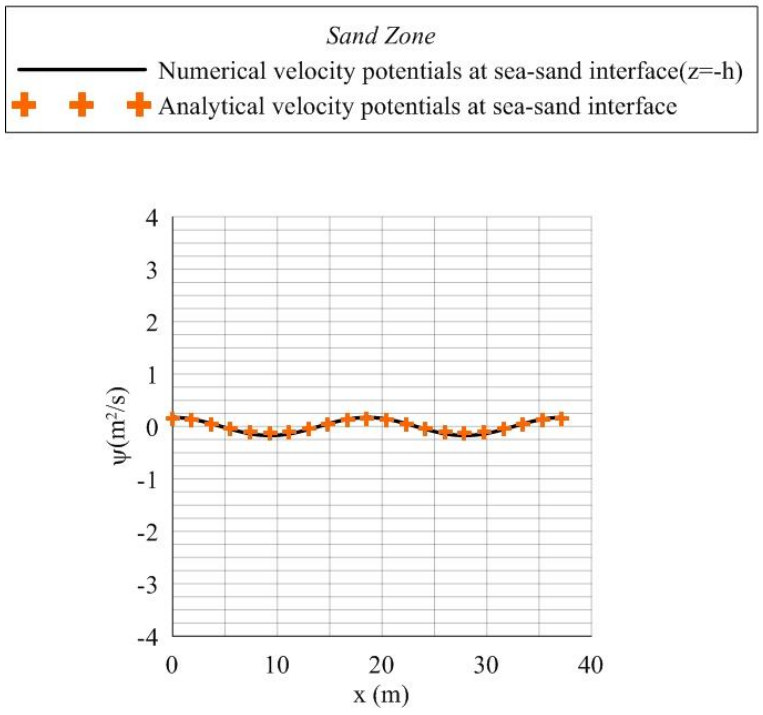

Figure 5.22. Velocity potentials in sand zone (z=-h).

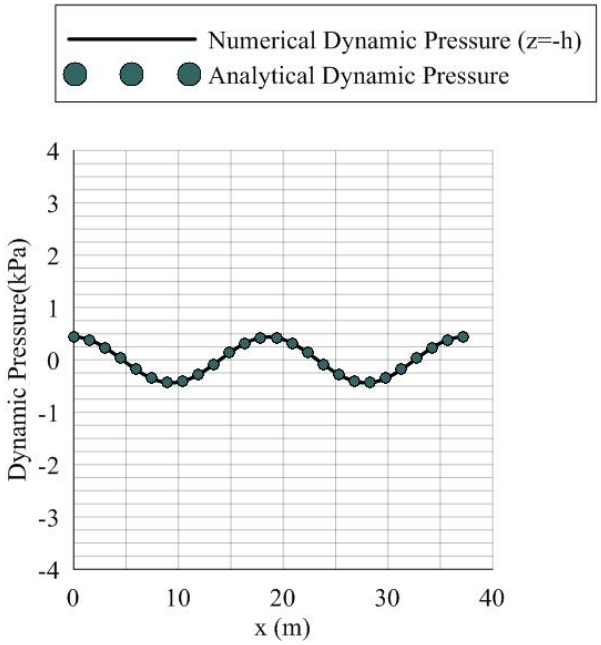

Figure 5.25. Dynamic pressures (z=-h).

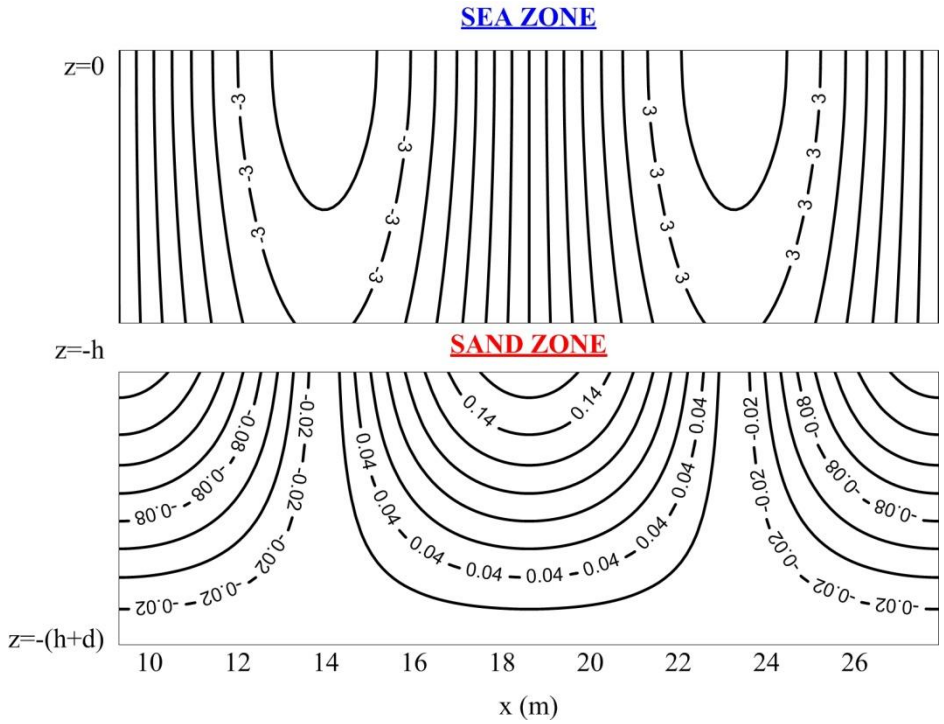

Figure 5.24. Contours of RBFCM interpolated velocity potentials.

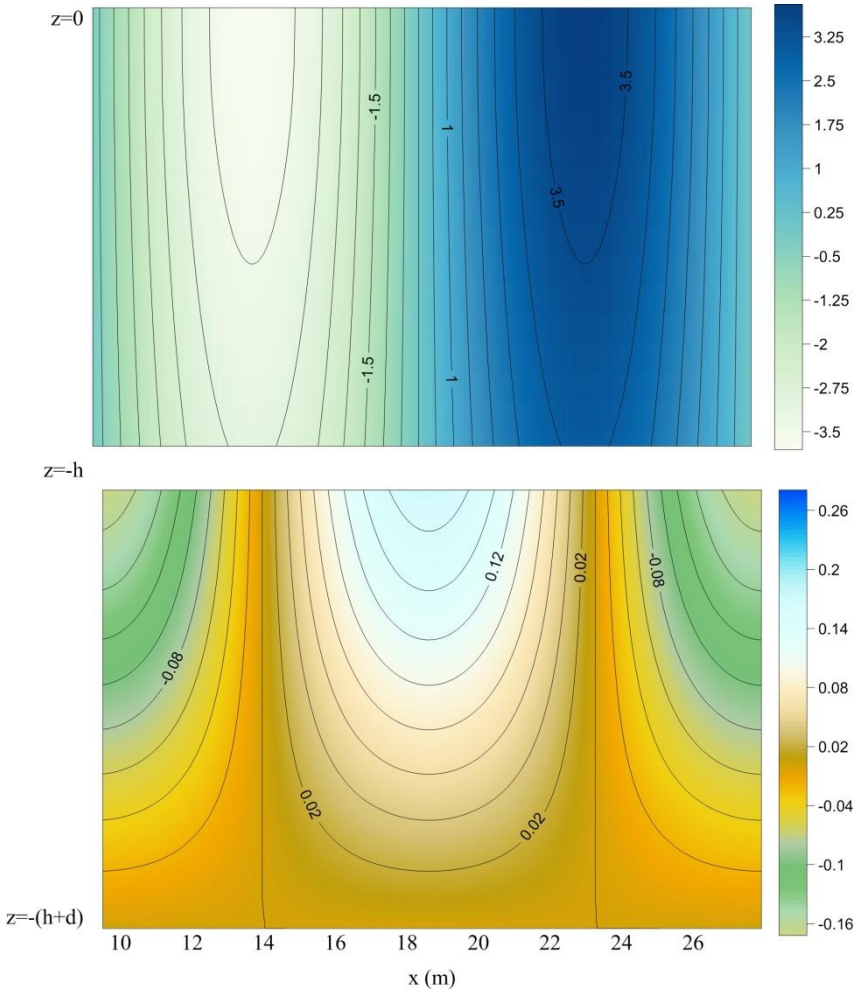

Figure 5.26. Image plots of velocity vectors inside sea and sand zones.

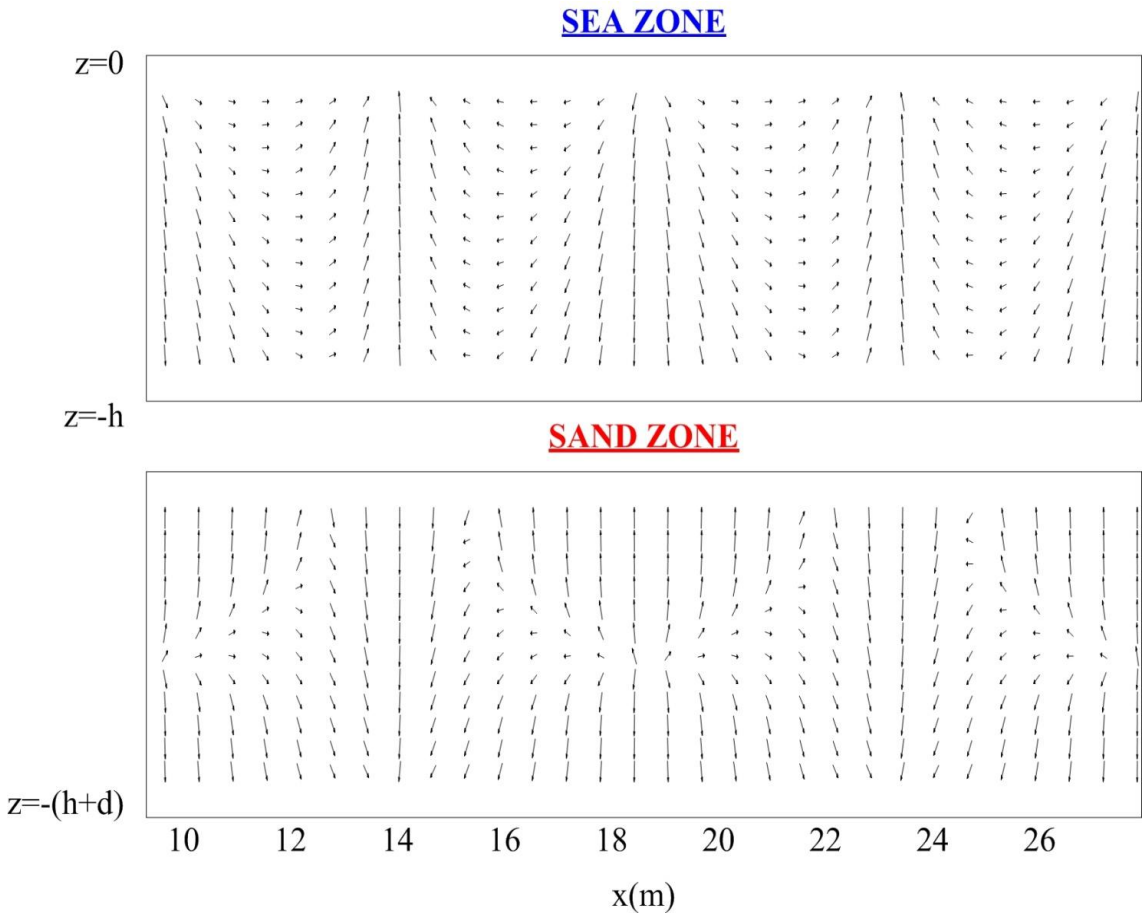

Figure 5.27. Velocity vectors.

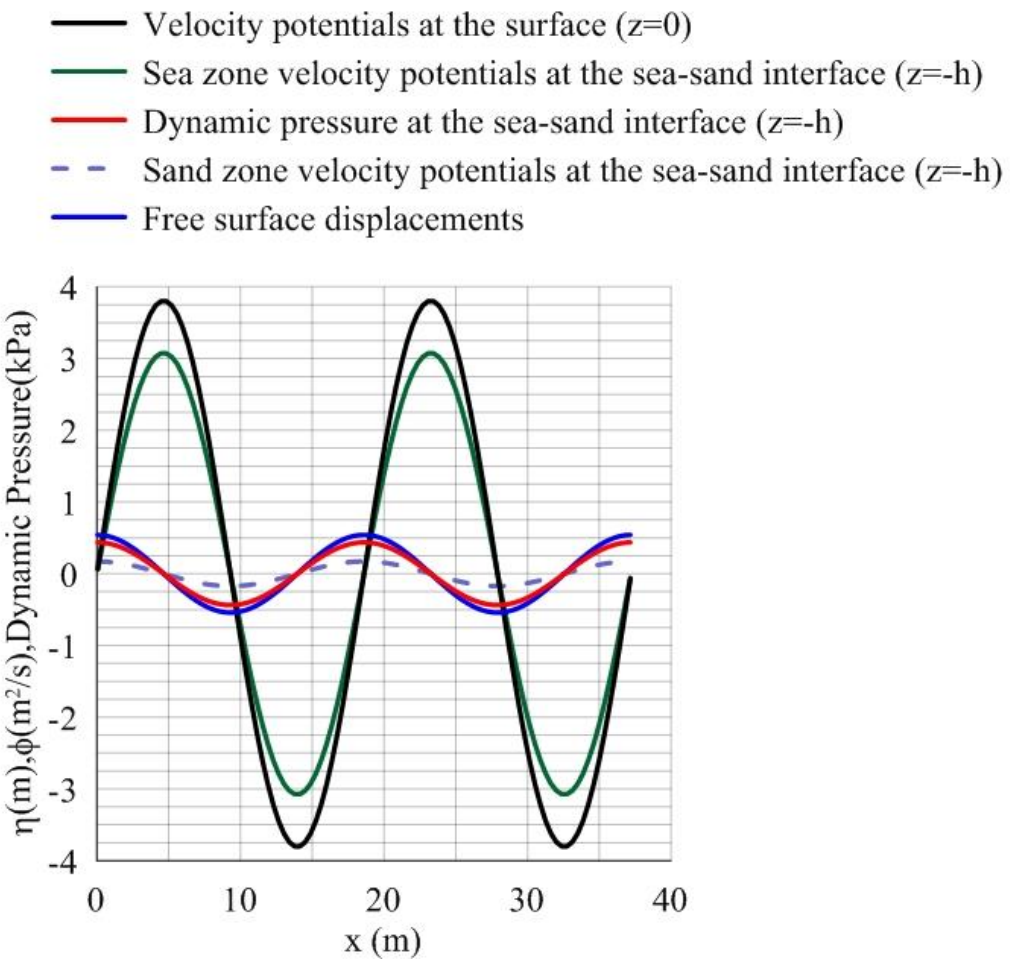

Figure 5.28. Numerical results for rippled and impervious sea bed.

5.6. Error Analysis for Shallow, Intermediate and Deep Water Depth Cases

Numerical results obtained and their comparison with the analytical solutions for the four stages of the present study so far, shows that the boundary type RBFCM is an efficient method to simulate the physical phenomenon at hand. However, the numerical simulation case presented so far, is for the intermediate water where $0.05 < d/L < 0.5$ (where d is the water depth and L is the wave length).

It should be verified that the present models are capable of simulating the cases for shallow water where $0 < d/L < 0.05$ and for deep water where $d/L > 0.5$. For accomplish this task, five kh cases in each of shallow, intermediate and deep are selected. For each case, the root mean square error (RMS) norm which is defined as,

$$e_{rms} = \sqrt{\frac{\sum_{i=1}^{N} (u_a - u_n)_i^2}{N}}$$

and the absolute error norm which is defined as,

$$e_a = |u_a - u_n|$$

are calculated. Five cases in each of shallow, intermediate and deep water can be found in Tables (5.9) to (5.11). Related error analysis plots are given in Figures 5.29 and 5.30.

Table 5.9. Shallow Water Cases

Case#	**Depth**	***T*(sec)**	***kh***	**H/L**	**d/L**	**H_o(m)**
1	1 m	7.5	0.271	0.066	0.043	1.1
2	1 m	9.0	0.225	0.060	0.036	1.1
3	1 m	10.0	0.210	0.056	0.032	1.1
4	1 m	12.0	0.168	0.051	0.027	1.1
5	1 m	15.0	0.134	0.0456	0.021	1.1

Table 5.10. Intermediate Water Cases

Case#	**Depth**	***T*(sec)**	***kh***	**H/L**	**d/L**	**H_o(m)**
1	7.5 m	7.5	0.805	0.018	0.128	1.1
2	7.5 m	9.0	0.651	0.015	0.104	1.1
3	7.5 m	10.0	0.579	0.014	0.092	1.1
4	7.5 m	12.0	0.474	0.012	0.076	1.1
5	7.5 m	15.0	0.375	0.011	0.060	1.1

Table 5.11. Deep Water Cases

Case#	**Depth**	***T*(sec)**	***kh***	**H/L**	**d/L**	**H_o(m)**
1	50 m	4.0	12.58	0.044	2.00	1.1
2	50 m	5.0	8.05	0.028	1.28	1.1
3	50 m	6.0	5.60	0.020	0.89	1.1
4	50 m	7.0	4.11	0.014	0.65	1.1
5	50 m	8.0	3.16	0.011	0.50	1.1

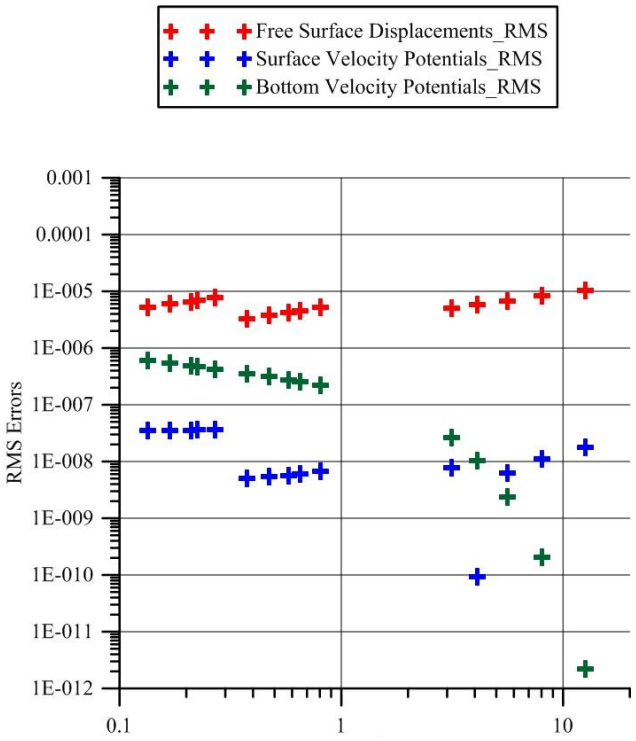

Figure 5.29. RMS errors for shallow, intermediate and deep water cases.

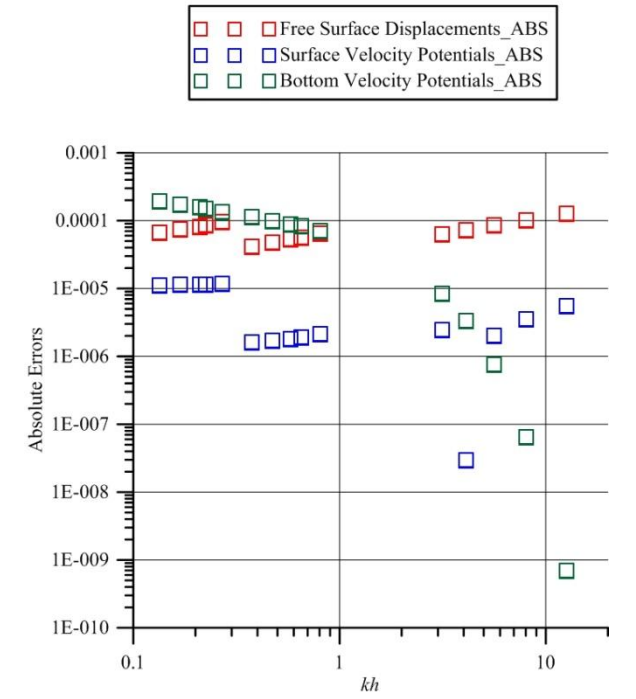

Figure 5.30. Absolute errors for shallow, intermediate and deep water cases.

Error analysis plots indicate that absolute errors are in range of $O(10^{-4})$ to $O(10^{-6})$ and the root mean square errors are in range of $O(10^{-5})$ to $O(10^{-9})$ for shallow, intermediate and deep water cases. These values are in tolerable range for a numerical model and they also indicate that the method used in the present study is an efficient method for simulating the wave propagation over pervious/impervious and horizontal/rippled sea bed.

5.7. Case Studies on Wave Dispersion Relation for a Pervious Sea Bed

In order to investigate the attenuation in the wave height due to the imaginary part of the wave number (obtained from the solution explained in sections 4.6 and 4.7), some case studies are done in this section.

In Figure 5.31, for a fixed sand layer thickness of 4 m, k_i values are plotted as a wave propagates from deep to shallow water (from $d = 20$m to $d = 1$m). Results show that the contribution of porosity to the damping of the wave height is negligible since k_i values are very small ($O(10^{-8}) \rightarrow O(10^{-11})$. ($T = 4.5$sec, $H_o = 1.1m$)

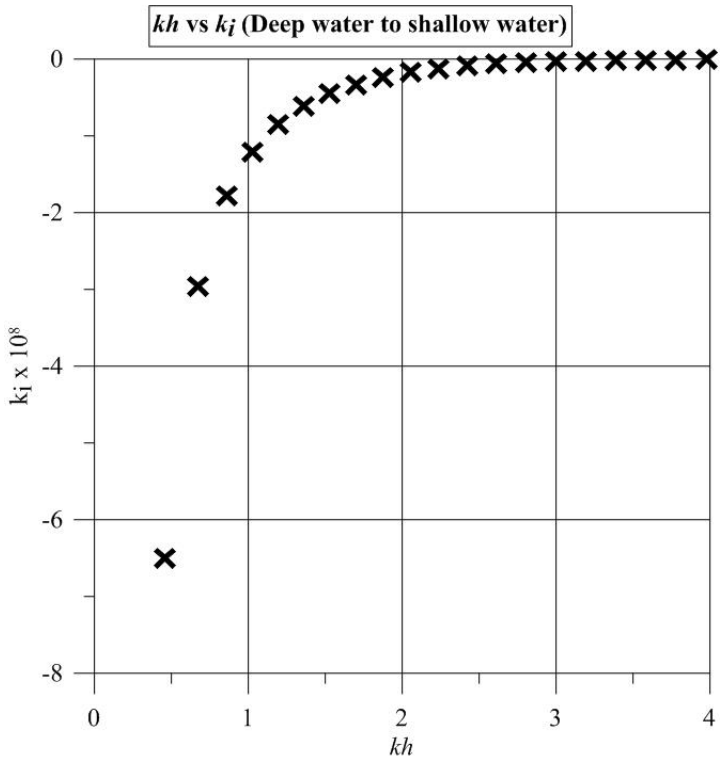

Figure 5.31. Variation of the imaginary part of the wave number from deep water to shallow water.

As waves move shore wards, they start to feel the pervious sea bed and k_i values increase due to the damping effect of porosity ($K = 10^{-6}$ m/s).

In Figure 5.32, the variation of k_i versus the sand layer thickness is plotted for a test wave with parameters; $T = 4.5\text{sec}, depth = 2\,m, H_o = 1.1m$. It is observed that k_i values vanish as the sand layer thickness increases. It can be concluded that $h = 20$ m can be regarded as an infinite sand layer thickness.

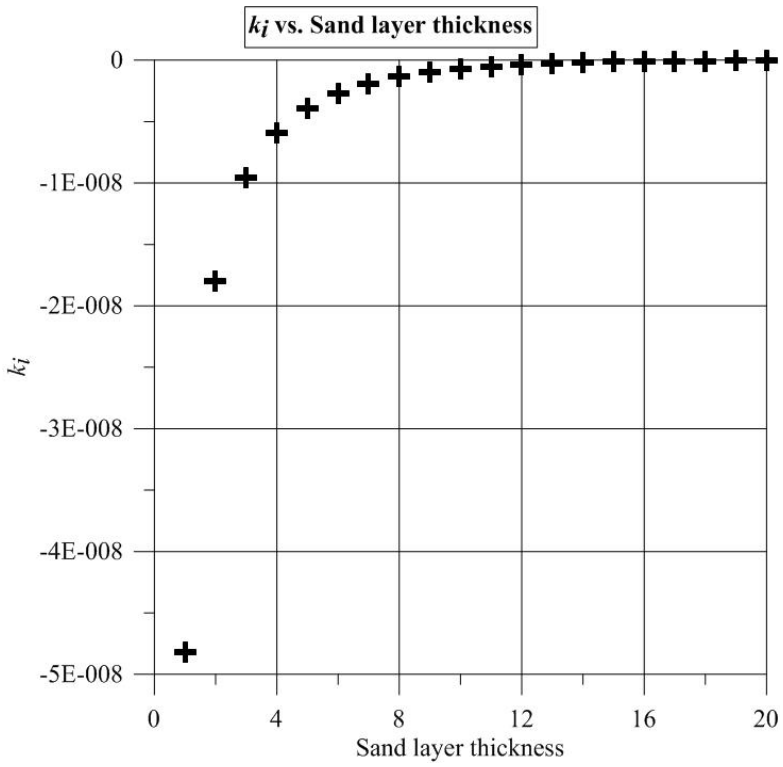

Figure 5.33. Imaginary part of the wave number variation with the sand layer thickness.

In Figure 5.33, analytical solution is utilized to plot the velocity potentials inside an infinitely thick sand layer ($h = 20$ m) for the wave parameters same as above. Figure 5.34 confirms the findings in Figure 5.33. Also, it can be observed that, in numerical results for a pervious sea bed presented so far, the contour distortion due to the unavailability of better lateral boundary conditions in the sand zone exists.

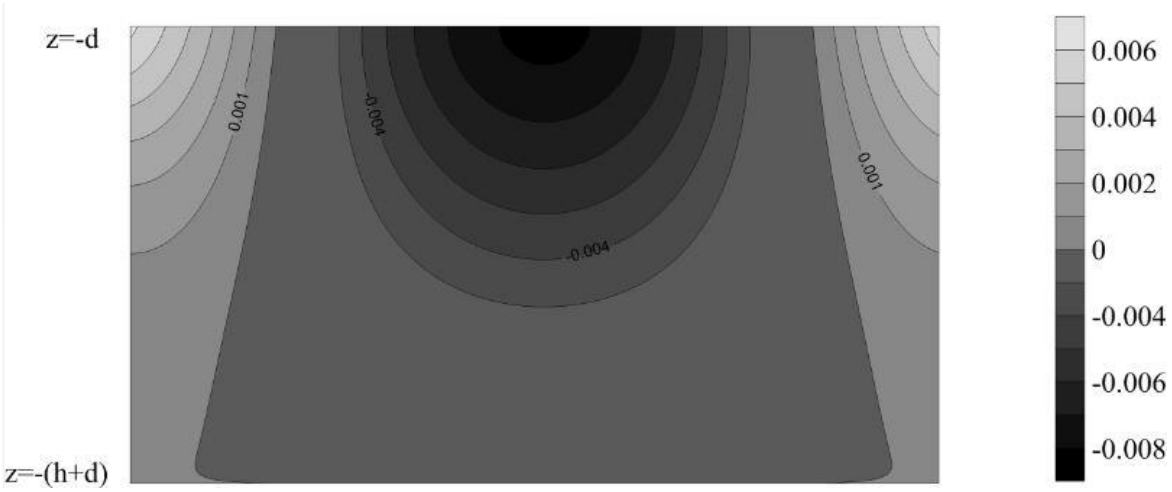

Figure 5.34. Contour plot of velocity potentials in an infinitely thick sand layer ($h = 20\,\text{m}$).

5.8. Verification of the RBFCM Interpolated Velocity Potentials

For the test case that is considered in Section 5.2, the RBFCM interpolated velocity over the depth of 2 m are plotted at different phases of the wave; $0, \pi/2$ and π including the surface and bottom velocity potentials. In Figure 5.34, these values are compared to the values obtained from the analytical solution at the same phases of the wave, in order to verify that RBFCM interpolation is efficiently capable of approximating the velocity potentials inside the solution domain. Figure 5.34 shows that, the RBFCM interpolation scheme used in this study is an efficient approximation method. RMS errors are found to be in range of 10^{-7} and 10^{-8}.

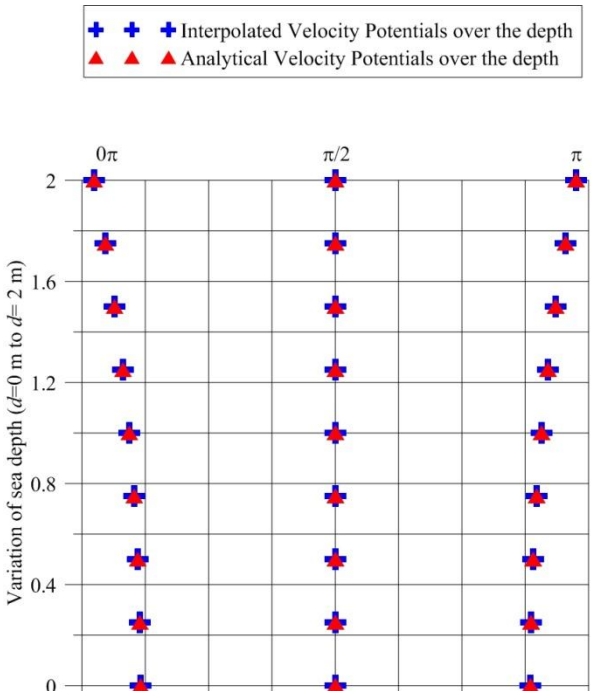

Figure 5.35. Comparison of interpolated velocity potentials with analytical solutions.

6. CONCLUSION AND FUTURE STUDIES

The aim of the proposed thesis work is the development of an understanding of how oxygen entrained in coastal waters penetrates into sandy sea bottoms. To understand the related phenomena, a linear wave propagation model over a porous sandy sea bed was developed using a meshless method, the Radial Basis Function Collocation Method (RBFCM). The Green's function of the Laplace equation was used as the Radial Basis Function (RBF). The solution of equations on the boundaries was used to obtain the values inside the solution domain using the RBF interpolation.

Numerical results and their comparison with analytical results and the error analysis in the present study indicate that the method used in this thesis study, a boundary type RBFCM, is an efficient method to solve the wave propagation problems over horizontal/rippled and pervious/impervious sea beds. It is clear that boundary-type RBFCM provides a quick and less time consuming (in terms of computational effort and computing time) work compared to the classical methods mentioned in earlier chapters. It should be noted that utilization of boundary-type RBFCM can handle various length scales with relatively smaller amount of nodes placed on the solution domain boundaries.

For the future study (understanding and modeling of oxygen transport inside a sandy sea bed) the models created in this thesis study form a solid basis. An advection-diffusion model can be coupled with the pervious sea bed models created and velocity vectors obtained here will be used as a basis for this. Yet, as mentioned in the beginning of the previous section, more reliable boundary conditions for the left and right boundaries of the sand zone should be provided.

For the rippled and impervious sea bed cases, a decrease in wavelength is observed when comparing the numerical and analytical results. For future studies, the effects of the ripples on wave parameters will be investigated.

Also, for the future study, a more complicated wave propagation model which covers terms such as friction, can be modeled in order to make a more realistic simulation of the problem at hand.

APPENDIX A: GREEN'S FUNCTION OF THE LAPLACE EQUATION

In this section, the derivation of the Green's function of the Laplace equation is given. We begin by considering the general second order linear partial differential equation in the dependent variable u and the two independent variables x and y ,

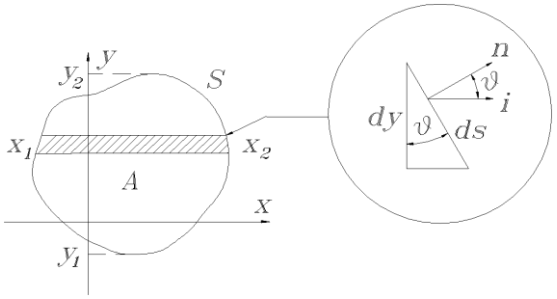

Figure A.1. Definition for integration by parts

$$Lu = a\frac{\partial^2 u}{\partial x^2} + 2b\frac{\partial^2 u}{\partial x \partial y} + c\frac{\partial^2 u}{\partial y^2} + d\frac{\partial u}{\partial x} + e\frac{\partial u}{\partial y} + fu = \phi \tag{A.1}$$

where $a, b, ..., f$ and ϕ are also known functions of the independent variables and the 2 is introduced for convenience. The equation above is to be solved in some region, A, subject to boundary conditions of the general form,

$$au + \beta\frac{\partial u}{\partial n} = h \tag{A.2}$$

prescribed on the boundary curve, S, of region A, α, β and h are functions along S and n denotes the outward normal. We now introduce the formal ad joint differential operator L^* associated with the operator L through the integral of the product vLu over the region of interest. All that we require of v is that it be continuous and differentiable to any order that we desire. Integrating the product repeatedly by parts yields a result of the general form,

$$\int_s vLudA = \int_s (f)ds + \int_A uL^* vdA \tag{A.3}$$

where the first integral represents boundary terms resulting from the integration performed along the bounding surface S. To illustrate the integration, consider integration of the first term of Equation (A.1),

$$\begin{aligned}
&\int_A va\frac{\partial^2 u}{\partial x^2}dA = \int_{y_1}^{y_2}\left\{\int_{x_1}^{x_2} va\frac{\partial^2 u}{\partial x^2}dx\right\}dy \\
&= \int_{y_1}^{y_2}\left\{va\frac{\partial u}{\partial x}\bigg|_{x_1}^{x_2} - \int_{x_1}^{x_2}\frac{\partial(av)}{\partial x}\frac{\partial u}{\partial x}\right\}dy \\
&= \int_{y_1}^{y_2}\left\{\left[va\frac{\partial u}{\partial x} - \frac{\partial(av)}{\partial x}u\right]\bigg|_{x_1}^{x_2} + \int_{x_1}^{x_2}\frac{\partial^2(av)}{\partial x^2}udx\right\}dy \\
&= \int_{y_1}^{y_2}\left\{\left[va\frac{\partial u}{\partial x} - \frac{\partial(av)}{\partial x}u\right]\bigg|_{x_1}^{x_2}\right\}dy + \int_A\frac{\partial^2(av)}{\partial x^2}udA \\
&= \int_S\left[va\frac{\partial u}{\partial x} - \frac{\partial(av)}{\partial x}u\right]\hat{i}.\hat{n}ds + \int_A\frac{\partial^2(av)}{\partial x^2}udA
\end{aligned} \tag{A.4}$$

Note that from Figure A.1, we have $dy = ds\cos\theta = ds\hat{n}.\hat{i}$, where ds is the differential element taken along S.

Integrating the remaining terms of the left hand side of Equation (A.3), we obtain,

$$\int_A vLudA = \int_S\left(M\hat{i} + N\hat{j}\right).\hat{n}ds + \int_A uL^*vdA \tag{A.5}$$

where,

$$\begin{aligned}
L^*v &= \frac{\partial^2(av)}{\partial x^2} + 2\frac{\partial^2(bv)}{\partial x\partial y} + \frac{\partial^2(cv)}{\partial y^2} + \frac{\partial(dv)}{\partial x} + \frac{\partial(ev)}{\partial y} + fv \\
M &= av\frac{\partial u}{\partial x} - u\frac{\partial(av)}{\partial x} + 2vb\frac{\partial u}{\partial y} + duv \\
N &= 2u\frac{\partial(bv)}{\partial x} + cv\frac{\partial u}{\partial y} + u\frac{\partial(cv)}{\partial y} + euv
\end{aligned} \tag{A.6}$$

As our interest is primarily in the solution of Laplace's equation, we now write Equation (A.5) with $a = c = 1$ and $b = d = e = f = \phi$ so that,

$$\begin{aligned}
M &= v\frac{\partial u}{\partial x} - u\frac{\partial v}{\partial x} \\
N &= u\frac{\partial v}{\partial y} - v\frac{\partial u}{\partial y}
\end{aligned} \tag{A.7}$$

Noting that,

$$(M\hat{i} + N\hat{j}).\hat{n} = (v\vec{\nabla}u - u\vec{\nabla}v).\hat{n} = v\frac{\partial u}{\partial n} - u\frac{\partial v}{\partial n} \tag{A.8}$$

Equation (A.5) becomes,

$$\int_A vLudA = \int_S \left(v\frac{\partial u}{\partial n} - u\frac{\partial v}{\partial n} \right) ds + \int_A uL^* vdA \tag{A.9}$$

where,

$$L^* v = \nabla^2 v \tag{A.10}$$

Equation (A.9) is a very important equation which will serve as the starting point of our development of the boundary element method for Laplace's equation. Before proceeding with the development, let us briefly discuss Equation (A.9) and what we intend to do with it. Recall that our aim is to determine u. The term on the left hand side of Equation (A.9) is zero since with $a, b, ..., f$ given as above we have,

$$Lu = \nabla^2 u = 0 \tag{A.11}$$

The first term on the right hand side is a line integral along the boundary and it involves the functions u and v as well as their derivatives normal to the boundary. It is through this term that we introduce the boundary conditions of the problem. Although we have not said anything about v, other than it being a continuous and differentiable function of x and y, let us assume that we know both v and its normal derivative at all points along S. The boundary conditions of the problem will specify either u or its normal derivative at each point along S. Therefore, there remains only one unknown at each point in the integral.

The last term of Equation (A.9), is an integral over the region A involving the unknown u and $L^* v$. As we shall see in what follows, a suitable choice of $L^* v$ will enable us to write an expression relating u and the line integral discussed above. This suitable choice is the two-dimensional Dirac delta function $\delta(x-\zeta, y-\eta)$, defined through the expression,

$$\int_A \delta(x-\zeta, y-\eta) f(x,y) dA = f(\zeta, \eta) \tag{A.12}$$

That is, the delta function is a generalized function which picks out the value of the function f at the point (ζ,η). It is also possible to visualize the delta function as the formal limit of a $\delta-$sequence, w_k (a sequence of ordinary functions which in the limit yields the delta function). Symbolically,

$$\delta(x-\zeta, y-\eta) = \lim_{k\to\infty} w_k(r) \tag{A.13}$$

where,

$$r = \sqrt{(x-\zeta)^2 + (y-\eta)^2} \tag{A.14}$$

A $\delta-$sequence suitable for our purpose here is given by,

$$w_k(r) = \frac{ke^{-kr^2}}{\pi} \tag{A.15}$$

Defined as above, the delta function represents a spike-like function of infinite height, vanishing width and unit area, centered at and having radial symmetry about the point (ζ,η).

Returning to our development, we first define the function v as our Green's function, G ,so that

Equation (A.9) becomes,

$$0 = \int_S \left(G\frac{\partial u}{\partial n} - u\frac{\partial G}{\partial n} \right) ds + \int_A uL^*G dA \tag{A.16}$$

Next, based on our discussion above we require,

$$L^*G = \nabla^2 G = -\delta(\zeta - x, \eta - y) \tag{A.17}$$

Note that the arguments of the delta function have been selected so that (x, y) denotes a fixed point in the solution domain and (ζ,η) are used temporarily as the independent variables. Also, a minus sign has been introduced before the delta function. These are merely conveniences so that Equation (A.15) becomes,

$$u(x, y) = \int_S \left(G\frac{\partial u}{\partial n} - u\frac{\partial G}{\partial n} \right) ds \tag{A.18}$$

Once we determine what our Green's function is by solving Equation (A.17), we may proceed to determine our solution $u(x, y)$, by evaluating the boundary integral in Eq. A.18.

To determine G, we first convert Equation (A.18) to polar coordinates in view of Equation (A.18) to Equation (A.15) (keeping in mind the limit process defined in Equation (A.13)),

$$\nabla^2 G = \frac{1}{r}\frac{\partial}{\partial r}\left[r\frac{\partial G}{\partial r}\right] + \frac{1}{r^2}\frac{\partial^2 G}{\partial \theta^2} = -\frac{ke^{-kr^2}}{\pi} \tag{A.19}$$

Since G depends only on r, its derivatives with respect to the angular coordinate are zero. This equation may now be integrated (after multiplying through by r) over a circular region from 0 to r,

$$r\frac{\partial G}{\partial r} = -\int_0^r \frac{k}{\pi} re^{-kr^2} dr = -\frac{1-e^{-kr^2}}{2\pi} \tag{A.20}$$

Dividing through by r and integrating once more yields,

$$G(r) = -\frac{1}{2\pi}\ln r + \lim_{k\to\infty}\frac{1}{2\pi}\int \frac{e^{-kr^2}}{r} dr \tag{A.21}$$

where the limit has been introduced in view of the definition of the delta function provided by Equation (A.13). The last term of the equation above tends to zero in the limit leaving,

$$G(r) = -\frac{1}{2\pi}\ln r;\ r = \sqrt{(x-\zeta)^2 + (y-\eta)^2} \tag{A.22}$$

which is the Green's function for the Laplace equation.

REFERENCES

Buhmann, M., *Radial Basis Functions: Theory and Implementation*, Cambridge University Press, Cambridge, UK, 2004.

Cheng, Y. Z., B. J. Chang, and Y. W. Yong, "A Coupled Numerical Model of Wave Interaction with Porous Medium", *Ocean Engineering*, Vol. 36, pp. 952-959, 2009.

Corvaro, S., A. Mancinelli, M. Brocchini, E. Seta, and C. Lorenzoni, "On the Wave Damping Due to a Permeable Sea Bed", *Coastal Engineering*, Vol. 57, pp. 1029-1041, 2010.

Cruz, E. C., M. Isobe, and A. Watanabe, "Boussinesq Equations for Wave Transformation on Porous Beds", *Coastal Engineering*, Vol. 30, pp. 125-156, 1997.

De Drezigue, O. D., D. Sous, and V. Rey, "Wave Propagation over a Steep Batymetric Slope: Influence of the Bed Porosity on the Wave Phase Matching", *Coastal Dynamics 2013*, pp. 421-430, 2013.

Dean, R. G., and R. A. Dalrymple, *Water Wave Mechanics for Engineers and Scientists*, 6th Ed., World Scientific, New Jersey, USA, 2000.

Dimas, A. A., and G. A. Kolokythas, "Flow Dynamics and Bed Resistance of Wave Propagation over Bed Ripples", *Journal of Waterway, Port, and Ocean Engineering*, Vol. 137, No. 2, pp. 64-74, 2011.

Hsiao, S. C., P. F. Liu, and Y. Chen, "Nonlinear Water Waves Propagating over a Permeable Bed", *Proceedings of the Royal Society Mathematical Physical & Engineering Sciences*, Vol. 458, No. 2022, pp. 1291-1322, 2002.

Hunt, J. N., "Direct Solution of Wave Dispersion Equation", *Journal of the Waterway Port Coastal and Ocean Division*, Vol. 105, No.4, pp. 457-459, 1979.

Hunt, J. N., "On the Damping of Gravity Waves Propagated over a Permeable Surface", *Journal of Geophysical Research*, Vol. 64, No. 4, pp. 437-442, 1959.

Kansa, E. J., "A Scattered Data Approximation Scheme with Applications to Computational Fluid Dynamics II Solutiuons of Parabolic, Hyperbolic and Elliptic Partial Differential Equations", *Computers and Mathematics with Applications*, Vol. 19, No. 8, pp. 147-161, 1990.

Kansa, E. J., "Multiquadrics - A scattered Data Approximation Scheme with Applications to Computational Fluid Dynamics I Surface Approximations and Partial Derivative Estimates", *Computers and Mathematics with Applications*, Vol. 19, No. 8, pp. 127-145, 1990.

Karunarathna, S. A., and P. Lin, "Numerical Simulation of Wave Damping Porous Sea Beds", *Coastal Engineering*, Vol. 53, No. 10, pp. 845-855, 2006.

Kim, G. W., and M. E. Lee, "Damping of Water Waves over Permeable Bed of Finite Depth", *Journal of the Korean Society of Marine Environment and Safety*, Vol. 18, No. 3, pp. 199-205, 2012.

Li, L., and D. A. Barry, "Wave-Induced Beach Groundwater Flow", *Advances in Water Resources*, Vol. 23, No. 4, pp. 325-337, 2000.

Liu, P. F., P. Lin, K. A. Chang, and T. Sakakiyama, "Numerical Modeling of Wave Interaction With Porous Structures", *Journal of Waterway, Port, Coastal and Ocean Engineering*, Vol. 125, No. 6, pp. 322-330, 1999.

Lui, P. F., "Damping of Water Waves Over Porous Bed", *ASCE Journal of Hydraulics Division*, Vol. 99, No.12, pp. 2263-2271, 1973.

Madsen, O. S., "Wave Induced Pore Pressures and Effective Stresses in a Porous Bed", *Geotechnique*, Vol. 28, No. 4, pp. 377-393, 1978.

Massel, S. R., "Circulaion of Groundwater due to Wave Set-up on aPermeable Beach", *Oceanologia*, Vol. 43, No. 3, pp.279-290, 2001.

McClain, R. C., N. E. Huang, and L. J. Pietrafesa, "Application of a Radiation-Type Boundary Condition to the Wave, Porous Bed Problem", *Journal of Physical Oceanography*, Vol. 7, No. 6, pp.823-835, 1977.

Moshagen, H., and A. Torum, "Wave Induced Pressures in Permeable Soils", *ASCE Journal of Waterways, Harbors and Coastal Engineering*, Vol.101, No. 1, pp.49-57, 1975.

Nielsen, P., *Some Basic Concepts of Wave Sediment Transport*, Inst.of Hydrodynamics and Hydraulic Engineering University of Denmark, Lyngby, Denmark, 1979.

Perrier, G., E. A. Hansen, C. Villaret, R. Deigaard, and J. Fredsoe, "Sediment Transport over Ripples in Waves and Currents", *Coastal Engineering*, Vol. 38, No. 10, pp. 2043-2057, 1994.

Pudjaprasetya, S. R., and I. Magdalena, "Wave Energy Dissipation over Porous Media", Vol. 7, No. 59, pp. 2925-2937, 2013.

Puri, K. K., "Viscous Damping of Gravity Waves Over Pemeable Bed", *International Journal of Mathematics and Mathematical Sciences*, Vol. 1, No.10, pp. 497-507, 1978.

Reid, R. O., and K. Kajiura, "On the Damping of Gravity Waves Over a Permeable Sea Bed", *Transactions - American Geophysical Union*, Vol. 38, No. 5, pp. 662-666, 1957.

Saks, S. E., "Gravity Waves in A Ponderable Flow With A Permeable Bottom", *Plenum Publishing Corporation*, Vol. 22, No. 2, pp. 263-264, 1987.

Salmon, J. R., P. F. Lui, and J. A. Liggett, "Integral Equation Method for Linear Water Waves", *Journal of The Hydraulics Division*, Vol. 106, No.12, pp. 1995-2009, 1980.

Shum, K. T., "The Effects of Wave-Induced Pore Water Circulation on the Transport of Reactive Solutes Below a Rippled Sediment Bed", *Journal of Geophysical Research*, Vol. 98, No. C6, pp. 10289-10301, 1993.

Shum, K. T., "Wave-Induced Advective Transport Below a Rippled Water-Sediment Interface", *Journal of Geophysical Research*, Vol. 97, No. C1, pp. 789-808, 1992.

Silva, R., E. Mendoza, and M. A. Losada, "Modelling Linear Wave Transformation Induced by Dissipative Structures (Regular Waves)", *Ocean Engineering*, Vol. 33, No. 16, pp. 2150-2173, 2006.

Silva, R., P. Salles, and G. Govaere, "Extended Solution for Waves Travelling over a Rapidly Changing Porous Bottom", *Ocean Engineering*, Vol. 30, No. 4, pp. 437-452, 2003.

Silva, R., A. G. L. Borthwick , and R. E. Taylor, "Numerical Implementation of the Harmonic Modified Mild-Slope Equation", *Coastal Engineering*, Vol. 52, No. 5, pp. 391-407, 2005.

Silva, R., P. Salles, and A. Palacio. "Linear Waves Propagating over a Rapidly Varying Finite Porous Bed." *Coastal Engineering*, Vol. 44, No. 3, pp.239-260, 2002.

Sleath, J. F. A., "Ripple Geometry Under Severe Wave Conditions", *Coastal Engineering*, Vol. 3, No. 27, pp. 2686-2699, 2000.

Sollitt, C. K., and Cross, R. H., "Wave Transmission Through Permeable Breakwaters", *Alpine Geophysical Associates Incorporation*, Vol. 1, No. 13, pp. 1827-1846, 1972.

Ting, C. L., M. C. Lin, and Y. C. Cheng, "Porosity Effects on Non-Breaking Surface Waves over Permeable Submerged Breakwaters", *Coastal Engineering*, Vol. 50, No. 4, pp. 213-224, 2004.

Tsai, C. P., Chen, H. C., and Lee, F. C., "Wave Transformation over Submerged Permeable Breakwater on Porous Bottom", *Ocean Engineering*, Vol. 33, No. 11, pp. 1623-1643, 2006.

Wu, N. J., Tsay, T. K., and Young, D. L., "Computation of Nonlinear Free-Surface Flows by a Meshless Numerical Method", *Journal of Waterway, Port, Coastal and Ocean Engineering*, Vol. 134, No. 2, pp. 97-103, 2008.

Wu, N. J., Tsay, T. K., and Young, D. L., "Meshless Numerical Simulation for Fully Nonlinear Water Waves", *International Journal for Numerical Methods in Fluids*, Vol. 50, No. 2, pp. 219-234, 2006.

Yamamoto, T., H. Koning, H. Sellmeijer, and E. Van Hijum, "On the Response of a Poro-Elastic Bed to Water Waves", *Journal of Fluid Mechanics*. Vol. 87, No. 1, pp. 193-206, 1978.

Zhu, S., "Water Waves within a Porous Medium on an Undulating Bed", *Coastal Engineering*, Vol. 42, No. 1, pp. 87-101, 2001.